



**UNIVERSIDAD DE INVESTIGACIÓN DE TECNOLOGÍA  
EXPERIMENTAL YACHAY**

**Escuela de Ciencias Biológicas e Ingeniería**

**TÍTULO: Impact of mono- and poly-saccharides on the ultrasound-mediated green synthesis of silver selenide nanoparticles**

Trabajo de integración curricular presentado como requisito para la obtención del título de Ingeniera Biomédica

**Autor:**

Armijo García Cinthya Daniela

**Tutor:**

Dahoumane Si Amar, Ph.D.

Urququí, julio 2020

**SECRETARÍA GENERAL**  
**(Vicerrectorado Académico/Cancillería)**  
**ESCUELA DE CIENCIAS BIOLÓGICAS E INGENIERÍA**  
**CARRERA DE BIOMEDICINA**  
**ACTA DE DEFENSA No. UITEY-BIO-2020-00023-AD**

A los 12 días del mes de junio de 2020, a las 15:00 horas, de manera virtual mediante videoconferencia, y ante el Tribunal Calificador, integrado por los docentes:

Presidente Tribunal de Defensa	Dr. SANTIAGO VISPO, NELSON FRANCISCO , Ph.D.
Miembro No Tutor	Dr. AVILA SOSA, EDWARD EBNER , Ph.D.
Tutor	Dr. DAHOUMANE , SI AMAR , Ph.D.

El(la) señor(ita) estudiante **ARMIJO GARCIA, CINTHYA DANIELA**, con cédula de identidad No. 0202584944, de la **ESCUELA DE CIENCIAS BIOLÓGICAS E INGENIERÍA**, de la Carrera de **BIOMEDICINA**, aprobada por el Consejo de Educación Superior (CES), mediante Resolución RPC-SO-43-No.498-2014, realiza a través de videoconferencia, la sustentación de su trabajo de titulación denominado: **IMPACT OF MONO- AND POLY-SACCHARIDES ON THE ULTRASOUND-MEDIATED GREEN SYNTHESIS OF SILVER SELENIDE NANOPARTICLES** , previa a la obtención del título de **INGENIERO/A BIOMÉDICO/A**.

El citado trabajo de titulación, fue debidamente aprobado por el(los) docente(s):

Tutor	Dr. DAHOUMANE , SI AMAR , Ph.D.
-------	---------------------------------

Y recibió las observaciones de los otros miembros del Tribunal Calificador, las mismas que han sido incorporadas por el(la) estudiante.

Previamente cumplidos los requisitos legales y reglamentarios, el trabajo de titulación fue sustentado por el(la) estudiante y examinado por los miembros del Tribunal Calificador. Escuchada la sustentación del trabajo de titulación a través de videoconferencia, que integró la exposición de el(la) estudiante sobre el contenido de la misma y las preguntas formuladas por los miembros del Tribunal, se califica la sustentación del trabajo de titulación con las siguientes calificaciones:

Tipo	Docente	Calificación
Miembro Tribunal De Defensa	Dr. AVILA SOSA, EDWARD EBNER , Ph.D.	10.0
Tutor	Dr. DAHOUMANE , SI AMAR , Ph.D.	10.0
Presidente Tribunal De Defensa	Dr. SANTIAGO VISPO, NELSON FRANCISCO , Ph.D.	10.0

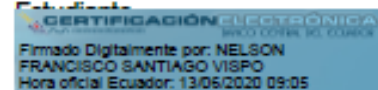
Lo que da un promedio de: **10 (Diez punto Cero)**, sobre 10 (diez), equivalente a: **APROBADO**

Para constancia de lo actuado, firman los miembros del Tribunal Calificador, el(la) estudiante y el(la) secretario ad-hoc.

*Certifico que en cumplimiento del Decreto Ejecutivo 1017 de 18 de marzo de 2020, la defensa de trabajo de titulación (o examen de grado modalidad teórico práctica) se realizó vía virtual, por lo que las firmas de los miembros del Tribunal de Defensa de Grado, constan en forma digital.*

**ARMIJO GARCIA, CINTHYA DANIELA**

Estudiante



CERTIFICACIÓN ELECTRÓNICA  
 Firmado Digitalmente por: NELSON FRANCISCO SANTIAGO VISPO  
 Hora oficial: Ecuador: 13/06/2020 09:05

Dr. SANTIAGO VISPO, NELSON FRANCISCO , Ph.D.

Presidente Tribunal de Defensa

**CERTIFICACIÓN ELECTRÓNICA**  
Firmado Digitalmente por: SI AMAR  
DAHOUMANE .  
Hora oficial Ecuador: 14/05/2020 21:12

**Dr. DAHOUMANE , SI AMAR , Ph.D.**

**Tutor**

**EDWARD  
EBNER AVILA  
SOSA**

Firmado digitalmente  
por EDWARD EBNER  
AVILA SOSA  
Fecha: 2020.06.15  
11:59:45 -05'00'

**Dr. AVILA SOSA, EDWARD EBNER , Ph.D.**

**Miembro No Tutor**



Firmado digitalmente por:  
**KARLA  
ESTEFANIA  
ALARCON FELIX**

**ALARCON FELIX, KARLA ESTEFANIA**

**Secretario Ad-hoc**

## AUTORÍA

Yo, **CINTHYA DANIELA ARMIJO GARCÍA**, con cédula de identidad 0202564944, declaro que las ideas, juicios, valoraciones, interpretaciones, consultas bibliográficas, definiciones y conceptualizaciones expuestas en el presente trabajo; así como, los procedimientos y herramientas utilizadas en la investigación, son de absoluta responsabilidad de el/la autora (a) del trabajo de integración curricular. Así mismo, me acojo a los reglamentos internos de la Universidad de Investigación de Tecnología Experimental Yachay.

Urcuquí, julio 2020.

Daniela Armijo

Cinthy Daniela Armijo García

CI: 0202564944

## AUTORIZACIÓN DE PUBLICACIÓN

Yo, **CINTHYA DANIELA ARMIJO GARCÍA**, con cédula de identidad 0202564944, cedo a la Universidad de Investigación de Tecnología Experimental Yachay, los derechos de publicación de la presente obra, sin que deba haber un reconocimiento económico por este concepto. Declaro además que el texto del presente trabajo de titulación no podrá ser cedido a ninguna empresa editorial para su publicación u otros fines, sin contar previamente con la autorización escrita de la Universidad.

Asimismo, autorizo a la Universidad que realice la digitalización y publicación de este trabajo de integración curricular en el repositorio virtual, de conformidad a lo dispuesto en el Art. 144 de la Ley Orgánica de Educación Superior

Urququí, julio 2020.



---

Cintha Daniela Armijo García

CI: 0202564944

## Dedicatoria

El mayor de los agradecimientos, a mis padres, por su apoyo y amor incondicional durante toda mi vida convirtiéndose en mi fortaleza y ganas de triunfar. Sin lugar a duda, sin ustedes no sería la mujer que soy ahora. Gracias por todo su esfuerzo y sacrificio, no me alcanzara la vida para agradecer y recompensar todas y cada una de las cosas que han hecho por nosotros. Mis hermanitos Melissa, Emili y Alejandro son el regalo más grande que la vida me dio. Gracias por ser mi alegría y mis ganas de superarme día tras día, ustedes son y serán las personas más importantes en mi vida.

Quiero agradecer de manera especial a mi prima Lis por siempre estar a mi lado celebrando mis victorias y dándome ánimos en las derrotas, eres una mujer increíble a la cual admiro y adoro con todo el corazón, espero que Dios nos permita compartir mil carnavales juntas.

A mis profesores y ex-profesores por su maravillosa labor como docentes e investigadores, gracias por sus enseñanzas y sobre todo por siempre velar por el bienestar de los estudiantes. A mi tutor Si Amar Dahoumane por ser mi mentor y mi guía durante el desarrollo de mi tesis, gracias infinitas por sus consejos y apoyo en los momentos difíciles.

A las personas más extraordinarias que Yachay Tech me dio la oportunidad de conocer. Gracias Kianny, Karen, Lore, Carlita y Danna por ser sin duda alguna las mejores amigas, confidentes y compañeras durante estos últimos 5 años. A José, Manu, Moises, Alejo y Roberto por brindarme su cariño y ser mi soporte durante los días difíciles. A Full Aguante por ser el mejor equipo, gracias chicas por siempre permanecer unidas, superándonos y sobre todo porque siempre prevaleció la amistad. Todos ustedes hicieron de Yachay un hogar, me llevo los mejores recuerdos y sobre todo valiosas lecciones de vida.

Infinitas gracias a todas las personas que formaron parte de mi vida durante mi paso por Yachay Tech. Amigos, compañeros, y de manera especial a Lupe mi compañera de laboratorio. Gracias por todos y cada uno de los momentos compartidos, los llevare siempre en mi corazón.

Cinthya Daniela Armijo García

## Acknowledgments

I would like to express my deepest gratitude to my tutor Si Amar Dahoumane, whose support and scientific guidance were invaluable in the development of this research. Furthermore, special thanks to the Yachay Tech professors Thibault Terencio, Edward Avila, and Carlos Reinoso for their patient and continuous support. In ESPE (Sangolqui, Ecuador) I'd also like to extend my gratitude to Alexis Debut and Karla Vizuite, whose expertise and dedication contributed to the obtainment of excellent final results.

This accomplishment would not have been possible without the support of all of them.

Cinthya Daniela Armijo García

# Resumen

Las nanopartículas de seleniuro de plata ( $\text{Ag}_2\text{Se}$ ) fueron sintetizadas con éxito mezclando nitrato de plata ( $\text{AgNO}_3$ ) y ácido selenoso ( $\text{H}_2\text{SeO}_3$ ) que actúan como fuentes de Ag y Se, respectivamente. En presencia de fructosa y almidón como agentes reductores y estabilizantes, respectivamente. El proceso mediado por la sonoquímica se realizó usando agua como solvente a temperatura moderada, satisfaciendo los principios de la Química Verde. Se realizó un estudio de detección sobre el impacto de los parámetros experimentales, como la naturaleza de los monosacáridos, las cantidades de mono y polisacáridos y el tiempo de reacción, sobre el tamaño, la forma y la estabilidad coloidal de las nanopartículas sintetizadas de  $\text{Ag}_2\text{Se}$  que, a su vez, impactan sus propiedades ópticas. La morfología de  $\text{Ag}_2\text{Se}$  NPs sintetizadas se ha caracterizado por microscopía electrónica de transmisión (TEM) y las fases  $\alpha$  y  $\beta$  del  $\text{Ag}_2\text{Se}$  se determinaron mediante la técnica de difracción de rayos X (XRD). Además, las propiedades ópticas de  $\text{Ag}_2\text{Se}$  se estudiaron mediante espectroscopia UV-Visible y el análisis elemental se realizó de forma no destructiva utilizando la técnica microscopía electrónica de barrido con EDS. En comparación con los métodos anteriores, el presente método ambientalmente benigno arroja luz sobre una ruta novedosa, simple y de bajo costo para sintetizar nanomateriales valiosos que pueden tener una amplia gama de bio-aplicaciones.

**PALABRAS CLAVE:** Química Verde, Seleniuro de Plata, Nanopartículas, Fructosa, Almidón, Sonoquímica.



## Abstract

Silver selenide ( $\text{Ag}_2\text{Se}$ ) nanostructures have been successfully synthesized by mixing silver nitrate ( $\text{AgNO}_3$ ) and selenous acid ( $\text{H}_2\text{SeO}_3$ ) acting as Ag and Se sources, respectively. In the presence of fructose and starch play the role of reducing and stabilizing agents, respectively. Sonochemistry-mediated process was performed using water as the solvent at mild temperature satisfying the principles of Green Chemistry. A screening study was carried out regarding the impact of experimental parameters, such as the nature of the mono-saccharides, the amounts of mono- and poly-saccharides, and reaction time, on the size, shape and colloidal stability of the as-synthesized  $\text{Ag}_2\text{Se}$  NPs which, in turn, impact their optical properties. The morphology of the as-synthesized  $\text{Ag}_2\text{Se}$  NPs has been characterized by transmission electron microscopy (TEM) and both  $\alpha$ - and  $\beta$ -phases of  $\text{Ag}_2\text{Se}$  were determined by X-ray diffraction (XRD) technique. Besides, the optical properties of  $\text{Ag}_2\text{Se}$  were studied by UV-Visible spectroscopy and the elemental analysis was performed non-destructively using SEM-EDS technique. Compared with previous methods, the present environmentally benign method sheds light into a novel, simple and low-cost route to synthesize valuable nanomaterials that may have a wide range of bio-applications.

**KEYWORDS:** Green Chemistry, Silver selenide, Nanoparticles, Fructose, Starch, Sonochemistry.

# Content

<b>Introduction</b> .....	1
Literature Review .....	2
Nanoscience and Nanotechnology.....	2
Silver selenide semiconductor nanoparticles .....	4
Nanofabrication methods.....	5
Green Synthesis.....	6
Reducing and Capping agents .....	7
Applications of Ag <sub>2</sub> Se nanoparticles .....	10
Problem Statement .....	12
General and Specific Objectives.....	13
<b>Methodology</b> .....	14
Synthesis of Ag <sub>2</sub> Se NPs .....	14
Sonication .....	14
Lyophilization/Freeze Drying .....	16
Instrumentation .....	17
Ultraviolet-Visible spectroscopy (UV-Vis).....	17
X-ray diffraction (XRD).....	18
Transmission Electron Microscopy (TEM) .....	20
Scanning Electron Microscopy (SEM) .....	21
<b>Results &amp; Discussion</b> .....	22
Experimental procedure .....	22
Materials. ....	22
Green synthesis of silver selenide NPs .....	22
Instrumentation .....	23
Visual results of Ag <sub>2</sub> Se NPs.....	23
UV-Vis study of Ag <sub>2</sub> Se NPs.....	25
XRD .....	27

TEM.....	29
SEM – EDS .....	32
<b>Conclusion &amp; Outlook .....</b>	<b>35</b>
Conclusions .....	35
Outlook .....	35
<b>Bibliography.....</b>	<b>37</b>

# Chapter 1

## Introduction

Nanoscience and nanotechnology involve research and technological developments at atomic, molecular, and macromolecular levels, providing fundamental knowledge to understanding phenomena and materials at the nanoscale. These technological developments result from the convergence of traditional fields of science under the same principle in order to create structures and functional systems with novel properties to improve the quality of life through sustainable development. The application of nanomaterials may bring significant enhancement in industry, agriculture, medicine, and the environment (1). Over the last two decades, the use of the nanoparticles has attracted particular attention due to their shape and size-dependent properties which differ from ones of their bulk counterpart. Among semiconductor nanomaterials, silver selenide ( $\text{Ag}_2\text{Se}$ ) is one of the most widely investigated chalcogenide materials due to its applications in electronics and biomedical field.  $\text{Ag}_2\text{Se}$  nanostructures are well-known to possess unique electronic and structural properties (2). Silver selenide typically exists as orthorhombic-phase with high electrical conductivity and, at a temperature above  $407^\circ\text{K}$ , as a cubic-phase with superionic characteristics. This phase transition is known to be a reversed process (3). High-quality  $\text{Ag}_2\text{Se}$  nanoparticles can be constructed by “top-down” techniques, producing very tiny structures from bulk materials through the physical manipulation of material. “Bottom-up” is the other approach to create nanostructures atom by atom or molecule by molecule. However, these complicated and expensive methods involve either toxic chemicals and high capital costs, generating hazardous toxic byproducts that are not environmentally friendly. As an alternative solution to this concern, the “Green chemistry” provides 12 principles as a guide in implementing less harmful synthesis (4).

The biosynthesis of nanoparticles that uses naturally occurring reductants and capping agents has caught the attention of the scientific community. Among these natural reagents, plant materials, microorganisms or their extracts have proven efficient in the synthesis of inorganic nanoparticles (NPs), usually in a nontoxic aqueous medium. The green synthesis of NPs provides advantages over the traditional physical and chemical methods as it is simple, cost-effective, with a renewable natural source, relatively easy to reproduce, and results in a more compatible and stable product (4). Many techniques have been employed in green technology, including biological methods, ultrasound energy, direct laser or microwave irradiation, or the use of Tollens reagent for the synthesis of controllable shape and size nanoparticles. However, nanoparticles are naturally unstable and tend to aggregate due to the onset of strong Van der Waals forces between particles (5). Reducing and capping agents provide stable passivation of the particle surface, preventing the agglomeration as well as the uncontrollable growth of particles. Among the materials used

as stabilizers, natural polymers provide an excellent steric hindrance effect along with potent stability (2). Besides, simple sugars, used as nontoxic reducing agents is a cheap and abundant natural source for the synthesis of inorganic NPs. This reducing character is achieved in their open-chain form and maximized with the ionization of the sugar (6). The green approaches are used to produce nontoxic and biocompatible nanoparticles applicable in the industry and biomedical field. Therefore, from a green chemistry perspective, three main steps in the preparation of nanoparticles should be consider: the solvent medium, reducing agent, and nontoxic stabilizing matrix (7).

The present work is focused on the green synthesis of silver selenide ( $\text{Ag}_2\text{Se}$ ) nanoparticles under sonochemical irradiation in aqueous solution. D-fructose is employed as the reducing and coprecipitating agent, replacing toxic and harmful agents, such as hydrazine, sodium borohydride, and dimethylformamide already reported in the literature. Finally, starch acts as a stabilizing agent offering like a template for the growth of the nanoparticles.

## Literature Review

### Nanoscience and Nanotechnology

Currently, nanoscience and nanotechnology play an important role in terms of scientific and industrial research and development. It's about scientific/technological disciplines dealing with the study, design, synthesis, and application of the matter at the nanometric-scale. When introducing Nanoscience and Nanotechnology concepts, it is important to distinguish the terms that compose them: "science" and "technology". The first is the ordered sets of knowledge that studies, searches and interprets natural, social, and artificial phenomena and the laws that govern these phenomena; the second refers to the set of instruments, methods, and techniques designed to solve specific problems. On the other hand, "nano" is a prefix unit that means "one-billionth part" ( $10^{-9}$ ). At this dimension, the physical, chemical and biological properties of materials change tremendously depending on their shape and size as well as their composition and structure (8). According to the Standardization International Organization (9), "nanoscale" is the range of sizes between "1 - 100 nm".

Although several possible definitions exist, a current and complete definition considers Nanoscience as the study of phenomena and manipulation of matter at atomic, molecular and macromolecular levels where the properties differ significantly from their bulk material. On the other hand, Nanotechnology is the design, characterization, production, and application of structures, devices, and systems, whose shape and size are controlled at a nonmetric-scale. Therefore, nanoscience is concerned with understanding effects such induced by features, such as size, surface tension or stickiness, and its influence on the

properties of the material. This fundamental knowledge is exploited by nanotechnology to create materials with desirable and novel properties (10,11).

It is not clear when humans began to take advantage of nanomaterials. It is known that in the 4<sup>th</sup> century A.D. glasses containing nanosized metals were fabricated by Roman glassmakers. An important piece from this period is the Lycurgus cup made from soda-lime glass containing gold and silver NPs, whose color changes from green to a deep red when a light source is placed inside (Figure 1a). Moreover, the variety of beautiful colors of the windows of the medieval cathedrals are due to metal NPs present in the glass (Figure 1b). In the 18<sup>th</sup> and 19<sup>th</sup> centuries, a photography film technology was developed that depended on the production of light-sensitive silver NPs. These films are an emulsion that contains silver halides which are broken down by the effect of the light source in the silver NPs becoming the pixels of the image. In the late 18<sup>th</sup> century George Eastman, who would later found the Kodak Corporation, made photography accessible to many by the manufacturing of a thin flexible film that could be rolled (12).

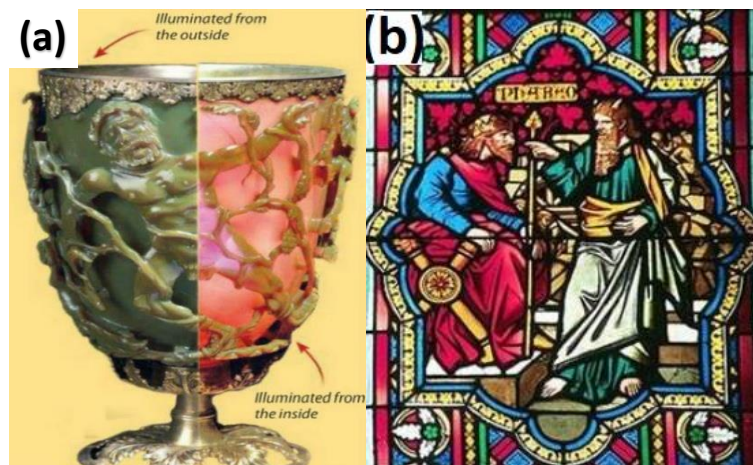


Figure 1: Image of (a) Lycurgus cup and (b) gothic stained glass window in Cologne Cathedral. Adapted from (5).

In 1960 Richard Feynman, a theoretical physicist at Caltech, first introduced the idea of nanotechnology at a meeting of the American Physical Society in his visionary speech, entitled "There is a lot of space at the bottom." Although, he never explicitly mentioned "nanotechnology," Feynman hinted that eventually, it would be possible to manipulate matter on a tiny scale to create a "nano-factories" (13). In 1979, inspired by Feynman's revolutionary ideas, Erick Drexler expanded the concepts of molecular fabrication towards the understanding of protein function. As a result, the field of nanotechnology was created (14). Ever since then nanotechnology has become an interdisciplinary field.

Nowadays, nanotechnology impacts the human daily life. This new technology involves chemists, physicists, biologists, and engineers under the same principle and method in the development of structures and functional systems with unique capabilities and potential benefits. Furthermore, it has become a foundation for different areas such as biomedicine, health care, industrial applications, and electronics. The in-depth study of nanomaterials and nanostructures is an important source for establishing new concepts, techniques and methods which yield the progress of science creating new opportunities for practical applications. (15,16).

### Silver selenide semiconductor nanoparticles

Among all semiconductor materials, silver chalcogenides have drawn immense attention by the scientific community due to their large spectrum of applications including biological/chemical sensors, solar cells, nanoscale electronic devices and catalysis (2). Semiconductor nanostructures often refer to as nanoparticles, quantum dots, nanocrystals, etc. They fall within the intermediate state of matter between the bulk phase and molecular regimen. Properties of nanomaterials can be modified by tuning their size giving rise to novel phenomena. In semiconductors, crystallite size is strongly related to their optical and electronic properties due to the increased surface area, so the quantum effects become progressively important with the reduction in size (17,18).

$\text{Ag}_2\text{Se}$  known as naumannite is a semiconductor material rarely found in nature as a mineral. It belongs to I-VI compounds with an optical band-gap between 1.2 and 1.8 eV (19). Silver selenide is a mixed ionic conductor with a phase transition at atmospheric pressure from a low-temperature orthorhombic phase ( $\beta\text{-Ag}_2\text{Se}$ ) with a narrow direct band-gap of 0.07 – 0.15 eV at 0 K, and a high-temperature cubic phase ( $\alpha\text{-Ag}_2\text{Se}$ , > 407 K) (20). The orthorhombic phase (Figure 2a -b) is the most accepted crystal structure of  $\text{Ag}_2\text{Se}$  due to its relative high Seebeck coefficient (thermoelectric power,  $-150 \mu\text{V/K}$ ) at 300 K, an unusually low lattice thermal conductivity coupled with high electrical conductivity (21).  $\beta\text{-Ag}_2\text{Se}$  compound exhibits photocatalytic activity and super hydrophobic characteristics; this compound has been used as a photosensitizer in photographic films, thermos-chromic materials for non-linear optical devices, and photovoltaic cells (22).

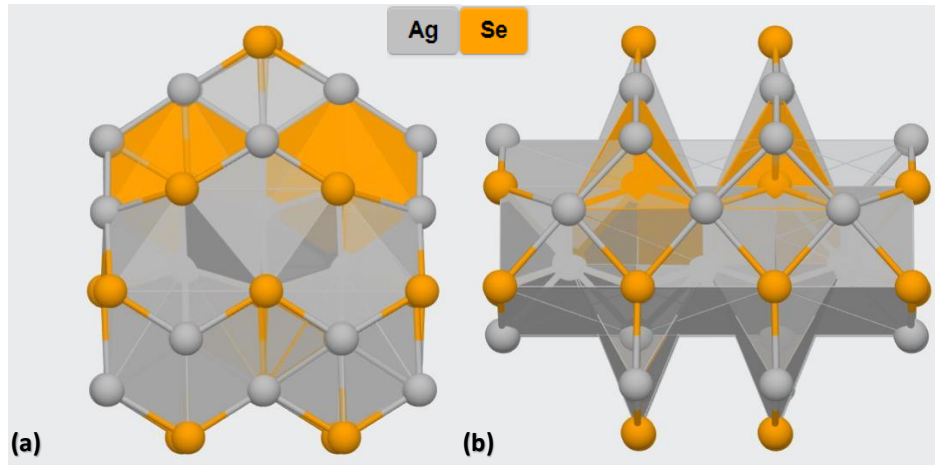


Figure 2: Orthonrhombic phase ( $\beta$ - $\text{Ag}_2\text{Se}$ ). (a) Frontal view and (b) lateral view. Adapted from (23).

## Nanofabrication methods

Physical manipulation of matter at nanoscale is the heart of nanoscience and nanotechnology. Nanofabrication aims to building structures at the atomic level in large quantities at a relatively low-cost. Nanofabrication methods can be divided into two main approaches: Bottom-up and Top-down methods.

### ➤ *Bottom-up methods*

Bottom-up approach deals with strategies to self-assemble and self-organize building blocks of atoms or molecules into multifunctional nanostructural materials through supramolecular interaction (i.e., hydrogen bonding, metal coordination, van der Waals, electrostatic,  $\pi$ - $\pi$ , hydrophilic-hydrophilic, and hydrophobic-hydrophobic interactions) in controlled chemical reactions (24). The result is a set of identically structures with fewer defects and homogenous chemical composition. The bottom-up approach has the potential to assemble functional multi-component devices, without waste or the need to develop or eliminate parts of the system. Some of the most prominent bottom-up methods include atomic layer deposition, sol-gel, molecular self-assembly, chemical vapor deposition, microemulsion (25).

### ➤ *Top-Down methods*

Top-down approach has evolved from the conventional lithography technology. The principle behind this method is to take a bulk material and modify or break it into desired structures; it normally involves cutting, grinding or etching out some materials to make the final ones. The key to these strategies is that the pieces are both patterned and built-in place, so no assembly step is needed (26). Top-Down approaches include various methods such as chemical etching (acids), mechanical etching (UV-light, X-rays, electron beams),



scanning probe lithography, nanoimprinting lithography, and block copolymer lithography (25).

### Green Synthesis

The biosynthesis of nanoparticles is essential in developing sustainable technologies, especially for the environment, due to its cost-effectiveness and eco-friendly character offering a serious alternative to chemical and physical methods. Green synthesis, based on the twelve principles of Green chemistry (27), interconnect nanotechnology and biotechnology for the synthesis of biocompatible stable NPs. Plant extracts, microorganisms, and viruses or their extracts are used as biological routes, due to their antioxidant and reducing properties for a large-scale production of NPs. Nanoparticles synthesized via green technology are superior to their counterparts obtained traditional methods thanks to diverse aspects, such as simple reproducibility, greater stability and appropriate dimensions. Furthermore, green technology consumes less energy, uses ecological, non-toxic and safe reagents generating environmentally benign products and byproducts (4).

#### ➤ *Biological method*

The potential of organisms in the synthesis of NPs ranges from a simple prokaryotic cell to eukaryotic cells and plants. Bio-based protocols have been followed for the synthesis of stable and well-characterized NPs considering critical parameters, such as kind and genetically properties of organisms, conditions of cell growth, enzyme activity, ideal reaction conditions, and the appropriate biocatalyst state. The morphology and size of the NPs can be controlled by substrates concentration, pH, temperature, light, reducing agent, and reaction time (28). These processes are divided into two categories depending where are formed NPs in the microorganisms. There are intracellular pathway, if the microorganisms promote the NPs in their inside or extracellularly pathway if production of the NPs is out of the microorganisms (29).

#### ➤ *Irradiation method*

Diverse kinds of radiations can be used to synthesize NPs. Direct laser irradiation technique produces well-defined NP populations in terms of shape and size, which can be altered by modulating the laser power. Particle size increases at low laser power in short reaction times, while it decreases at high laser power (30).

Microwave irradiation method is a less-time consuming approach for the production of NPs with a low size dispersion, although a precise control in morphology is not achieved (31).

Microwaves act as high-frequency radiation fields, which are capable of heating any material that contains electrical charges such as polar molecules or conductive ions. Conductive and semiconductor samples heat up when the ions and electrons they contained form an electric current and energy losses due to the electrical resistance of the material. Moreover, liquid solutions produce a decrease in temperature fluctuation medium, providing a homogeneous environment for the NP nucleation and growth (32).

➤ *Sonochemical method*

Ultrasound energy has been widely used to generate particles of a much smaller size and higher surface area than those reported by other methods. The chemical effects of ultrasound energy arise from acoustic cavitation, i.e. the formation, growth, and collapse of bubbles in a liquid. The bubble collapse generates a localized hotspot through adiabatic compression or shock wave formation within the gas phase of the collapsing bubble. The extreme conditions formed in the hotspots have been experimentally determined, the temperature of ~5000 K, pressures of 1800 atm, and cooling rates of 10 K/s. These extreme conditions could be advantageous for the fabrication of materials with different structures and properties (33).

➤ *Tollens method*

A simple one-step process, the Tollens method has been used for the synthesis of controlled NPs. This technique involves the reduction of a precursor (i.e. Tollens reagent) by an aldehyde. In the modified method, the controlled size and shape are directly proportional to the ammonia concentration, and the nature of the reducing agent. Thus, reducing agent and lowest ammonia concentration resulted in the smallest particle size with an intense maximum plasmon absorbance (28,34).

**Reducing and Capping agents**

➤ *Starch as a protective agent*

Starch is a widely available biopolymer that occurs in nature as semicrystalline granules. Starch granules have a complex structure comprising both crystalline and amorphous regions. Starch is a complex homopolymer composed of two polysaccharides, amylose and amylopectin. They are built of  $\alpha$ -D-glucopyranosyl units but differ in both structure and function (35). The relative weight percentage of amylose and amylopectin in natural starch

differ between 18% to 33% amylose and 72% to 82% amylopectin. However, high-amylose starch contains ~70% amylose, unlike genotypes which contain less than 1% (36).

Amylose (Figure 3a) is a linear polymer of (1→4) linked  $\alpha$ -D-glucopyranosyl residues with the average molecular mass of  $\sim 10^2$  to  $10^3$  kg mol<sup>-1</sup> (35). Ideally, the linear fraction consists of molecules structurally identical, varying only in the chain length (37). Amylopectin (Figure 3b) is a highly branched polysaccharide composed of hundreds of short  $\alpha$ - (1→4)- glucose chains, interlinked through  $\alpha$ - (1→6)-bonds. The molecular mass of amylopectin is around  $10^5$  kg mol<sup>-1</sup>. Amylopectin molecules differ in molecular size, number and length of branches per molecule, distances between them and the arrangement of branches into a pattern (35,36).

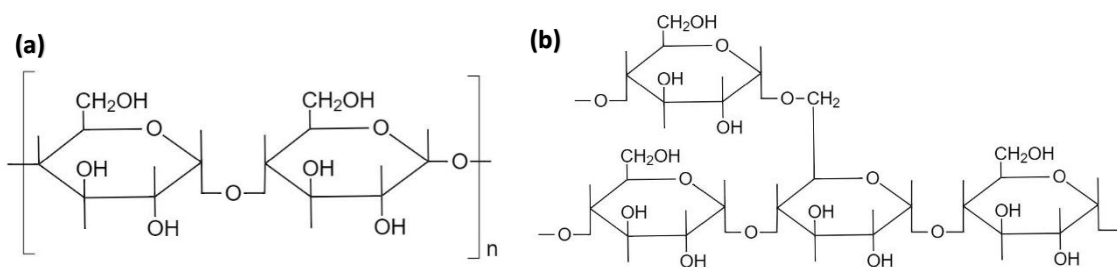


Figure 3: Chemical structure of (a) Amylose and (b) Amylopectin.

Natural starch exhibits several crystalline structures that differ in the packing density of the single or double helices and water content (37). The amylose fragment is associated with two polymorphic forms, the so-called A- and B-types, which consist of parallel double-stranded helices, right-handed or left-handed with parallel or antiparallel packing. Each turn of the helix contains six  $\alpha$ -D-glucose units (38). C-structure can be considered as a mixture of both A- and B-type polymorphs. Besides, in natural starch, a V-type structure is formed by amylose-lipid complexes. The chain conformation consists of a single helix left-handed and six glucose units per helix turn (35,36). The relative amount of crystalline structures is influenced by the ratio of both amylose and amylopectin, molecular mass, length of the external chains of amylopectin, degree of branching and therefore, the origin (37).

Starch as a “green” capping agent is the best candidate for the environmental benign synthesis of nanoparticles because it provides stable passivation of the surface preventing the aggregation of the nanoparticles. Starch, in particular, amylose, act as a protective polymer influencing the particle size and morphology of the resulting NPs (39). Biodegradable and biocompatible nanomaterials based on starch or starch mixture with polymers are readily available and can be widely used by nanotechnology and implemented in the food industry, agriculture and biomedical fields (40).

➤ *Simplest sugars as reducing agents*

Monosaccharides are single carbon chains of 3 to 7 in length with various adjacent hydroxyl groups (Table 1). The general structure or molecular formula is  $C_x(H_2O)_y$ , hence the name of carbohydrates.

Table 1: Monosaccharides

	Trioses	Tetroses	Pentoses	Hexoses	Heptoses
Carbon atoms	3	4	5	6	7

Hexoses, such as glucose and fructose can exist in isomeric form due to the oxidation of a hydroxyl group into a keto (ketones) or aldehyde (aldoses) groups (41,42). Structurally, monosaccharides of five or six carbon units can occur in both straight-chain form and cyclic form, the so-called furanose and pyranose rings, respectively. Carbohydrates and some organic compounds display stereoisomerism and optical isomerism. Stereoisomers, have the same molecular formula but a different arrangement of atoms in the space whereas, optical isomer have non-superimposable mirror images (enantiomers). Stereoisomers that are not enantiomers are called diastereomers (41,42). Carbohydrates have the conformation D- or L- depending on the orientation of the OH group of the chiral carbon.

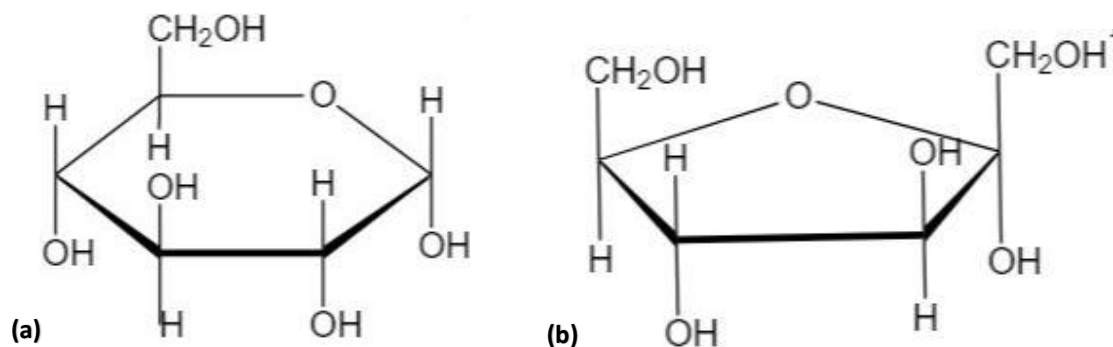


Figure 4: Chemical structures (a) D-Glucose and (b) D-Fructose.

D-Glucose can form  $\alpha$ - or  $\beta$ -D-glucopyranose configuration when the oxygen of the OH group of the 5<sup>th</sup> carbon adds to the carbonyl carbon to form a hemiacetal (Figure 4a). Fructose, a six-carbon ketose forms five-membered fructofuranose rings. D-fructose form  $\alpha$ -D-furanose configuration when the oxygen of the OH<sup>-</sup> group binds with C2 producing a hemiketal (Figure 4b) (42).

A reducing sugar contain a great variety of hydroxyl and carbonyl groups; these groups provide carbohydrate-coated NPs a unique H-bonding capability in assembling to a

supramolecular architecture (7). The reducing character of sugars is achieved by reacting with water to give rise to the open-chain form containing the aldehyde group. Thus, mono- and disaccharides are renewable, inexpensive, non-toxic reducing agents for the green synthesis of nanoparticles.

#### Applications of Ag<sub>2</sub>Se nanoparticles

##### ➤ *Photovoltaic devices*

Quantum confinement in nanocrystals induces unique optic and electronic properties that enhance the conversion of energy in the production of renewable cost-effective solar fuels (H<sub>2</sub>, CO, CH<sub>3</sub>OH, C<sub>x</sub>H<sub>y</sub>O<sub>z</sub>, C<sub>n</sub>H<sub>2n+2</sub>) (43). Quantum dot-based solar cells have the ability to convert sunlight into electricity (clean energy). However, the limitations encountered with photovoltaic devices are conversions efficiencies. The most effective way to overcome these limitations is to combine polymers with inorganic semiconductors, providing an interface for efficient charge transfer because of the nanoscale nature of light absorption and photocurrent generation in solar energy conversion (44). Nanostructured-photovoltaic devices exhibit several advantages such as energy saving, high efficiency, and high stability which make them more and more useful in many applications.

##### ➤ *Light-emitting devices*

Recent advances in quantum dots as alternative light-emitting elements and processing technologies have enabled numerous photonic applications to become a reality. Quantum dot-based light-emitting diodes (QLEDs) can have their color properties tuned by simply changing the size of the quantum dot used (45). This unique capability to use a single material for a range of different colors could present a cost-savings measure on an industrial scale. The most promising application is the flat-panel display technology, due to the advantages of solid-state, self-emission, full-color capability and flexibility of QLEDs encapsulated within organic polymers (16).

##### ➤ *Catalysts*

Nanoparticles have a high specific surface area (m<sup>2</sup>/g) which provides a higher catalytic activity. Nanotechnologies allow synthesizing metal NPs in solution in the presence of a surfactant to form highly monodispersed films of the catalyst NPs on a support structure. This approach enables more uniformity in the size and chemical structure of the as-

synthesized NPs, which in turn enhance the catalytic activity and reduce the generation of by-products. Also, it is possible to engineer NPs with specific or selective activity (10).

### ➤ *Biological Applications*

The advent of nanotechnology in the field of health sciences gives rise to a large number of diagnostic and therapeutic applications. Nanomedicine is the scientific revolution and technology of the 21<sup>st</sup> century, with economic implications that exceed 100 billion euros (46). Today, humanity is experiencing a progressive increase in diseases such as diabetes, Alzheimer's, Parkinson's, cancer and cardiovascular pathologies. Treatments for such diseases are expensive and remain ineffective in advanced stages. Nanomedicine is shown as an alternative in the search for new and rapid diagnostic and therapeutic methods that are efficient and specific at low cost. The most significant scientific advances within nanomedicine are:

#### *Nanodiagnosis*

The medical diagnosis using nanosystems has allowed an effective detection of diseases or cellular malfunction *in vivo and in vitro* (47), allowing the design of customized treatments for specific diseases, increasing therefore the patient's chances of recovery (48). In diagnostic nanosystems used *in vivo*, the biocompatibility of the material and its stability in physiological conditions play an important role when interacting with a certain pathogen or cancer cell avoiding its function being altered by the host's defenses. On the other hand, *in vitro* systems exhibit greater design flexibility, in less time, high sensitivity and precision.

Quantum dot labels have been successfully used in a wide number of bioanalytical purposes, such as immunoassays, DNA detection and binding assays using fluorescent tags for targeting molecules. Fluorescence immunoassays detect the binding between fluorescent-biomarker and the analyte molecule attached to a substrate. QDs-biomarkers have been successfully used as a substitute for organic fluorophores and colorimetric reagents in the detection of specific protein as well as cells of interest in immunoassays. Also, they could enable the detection of hundreds to thousands of molecules simultaneously (49).

### *Controlled drug delivery systems*

The biggest disadvantage of therapeutic drugs is the low specificity, causing damage to healthy tissue that are adjacent to the affected cells. Nanotherapy or controlled drug delivery systems aims at developing a vehicle (functionalized NP) which contains both therapeutic agents and recognition elements to locate and release drugs exclusively in affected cell areas, minimizing side-effects. Besides, these systems protect the drug from degradation before reaching the site of action. In this way, the administered doses could be lowered while keeping the same efficacy or even improving it (48).

## Problem Statement

The production of inorganic nanoparticles is currently of great interest to the scientific community as a result of scientific and technological advances in different fields. Due to these advances and the growing demand of nanomaterials in the modern industry, there is an increasing need to synthesize nanomaterials while considering the environmental aspects.

"Greener" processes or biosyntheses are a revolutionary alternative in response to environmental pollution problems associated with toxic wastes and byproducts generated by conventional methods which require and/or give rise to toxic substances. The twelve principles of Green Chemistry have become the base guide for the design and development of environmentally-benign and sustainable methodologies, through the use of renewable, biodegradable, and biocompatible reagents which, in turn, reduce the toxicity of the newly synthesized nanomaterials and the impact of their byproducts on the health and the environment.

To achieve this goal, the implementation of techniques, such as sonochemistry, is crucial in the development of new methodologies. The effects produced by the ultrasound are due to the creation, expansion, and explosion of small bubbles (cavitation) in the irradiated liquid. The cavitation phenomenon induces high temperatures and pressures in defined spots, conditions that promote chemical reactions. The ultrasound radiation favors the rate of the reaction, reduces the production of waste and unwanted byproducts, avoids purification processes, and improves the yields of the products in wet conditions.

In this context, this project proposes the green synthesis of semiconductor nanoparticles of silver selenide, using mono- and poly-saccharides as reducing and stabilizing agents, respectively, and the extensive characterization of their corresponding optical, structural and chemical properties using instrumental analysis techniques.



## General and Specific Objectives

### *General objective:*

To perform the green synthesis and characterization of silver selenide ( $\text{Ag}_2\text{Se}$ ) semiconductor nanoparticles using fructose and starch as reducing and stabilizing agents, respectively, under ultrasonic irradiation and perform their full characterization from chemical, structural, morphological and optical points-of-view.

### *Specific objectives:*

- To synthesize and characterize  $\text{Ag}_2\text{Se}$  NPs with controlled size and morphology, using the ultrasound technique.
- To investigate the impact of the concentration of the reducing agent on the size and the shape of the  $\text{Ag}_2\text{Se}$  NPs.
- To characterize the optical properties of these  $\text{Ag}_2\text{Se}$  NPs using UV-Vis spectroscopy, their size and shape using transmission electron microscopy, and their structural and crystalline features using X-ray diffraction.
- To determine the elemental composition of  $\text{Ag}_2\text{Se}$  NPs using a SEM-EDS.

# Chapter 2

## Methodology

### Synthesis of Ag<sub>2</sub>Se NPs

The Ag<sub>2</sub>SeNPs were prepared in a colloidal solution; thus a well-known and efficient method was employed. Ultrasonic synthesis method applies sound energy for an effective dispersion of Ag<sub>2</sub>SeNPs within the liquid phase. The application of ultrasound waves to nanomaterials improve the colloidal synthesis of uniform and highly crystalline NPs. Next, the sonication-assisted method is explained in detail.

#### Sonication

Sonication is an energy-efficient and cost-effective tool, widely used in toxicological and environmental applications to powder fragmentation or re-disperse stock suspensions to their nanoscale components. However, the erratic application of ultrasonic treatments, combined with a non-standardized process can influence the variability of the final result producing complex physical and chemical phenomena.

For a better understanding, some relevant terms are presented. *NPs* are defined as ultrafine particles with size-dependent properties, characterized by having at least one dimension ranging from 1 nm to 100 nm. A *Primary particle* is a subatomic entity which may form larger particle structures. There are two kinds of larger particle structures: aggregates and agglomerates. An aggregate is a collection of several primary particles, strongly fused, sintered or metallically bonded, whose bonds are difficult to break down. On the other hand, an agglomerate is a junction of primary particles and/or smaller aggregates by weak bonds. Therefore, agglomerates can be separated using sonication energy in order to obtain primary particles. The dissociation of agglomerates in a solvent creates a colloidal suspension where the particles are homogeneously distributed.

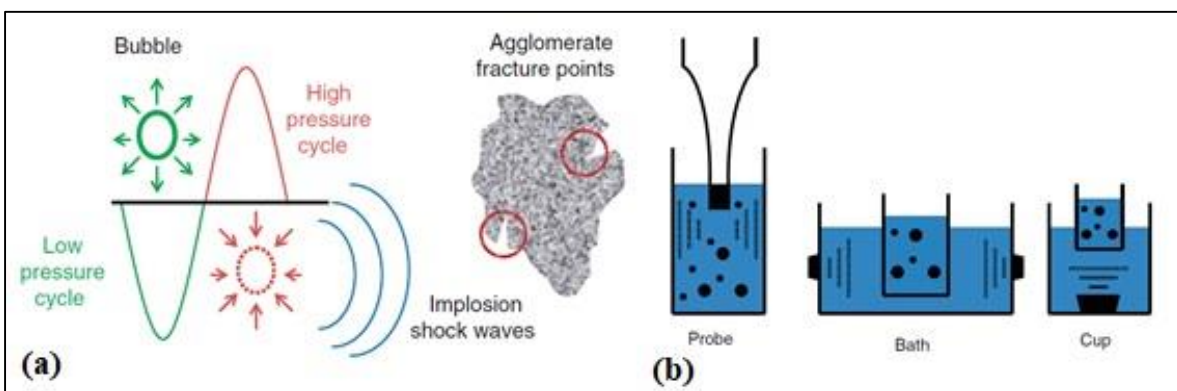


Figure 5: Graphical description of (a) cavitation process and (b) sonication configurations. Adapted from (50).

The sonication process is generated by sound waves that propagate through the liquid media in alternating low- and high-pressure cycles, generally in a frequency range between 20-40 kHz. During the low-pressure cycle known as rarefaction, microscale vapor bubbles are formed due to the cavitation process shown in Figure 5a. The created bubbles are dissociated during the high-pressure cycle (compression) generating a local shock wave that delivers a great amount of mechanical and thermal energy. There are various forms in which ultrasonic waves are generated. For example, direct immersion of the probe into the suspension (direct sonication) reducing the physical barriers to wave propagation, or introducing the sample in a bath or cup horn (indirect sonication) where the sound waves travel through the liquid medium as show in Figure 5b. The ultrasonic device produces vibrational energy from electrical power with the use of a piezoelectric transducer. This transducer responds with a change of volume when AC current is applied. The oscillation frequency in some cases is fixed by the device. Thus, a change in the instrument power configuration produces a change in the amplitude of the probe. The power value presented on the instrument display reveals the consumed power from the electrical source. But, the consumed power does not reflect the amount of power released to the medium. The power consumption in some systems is self-adjusted in order to keep the vibrational frequency at a constant value depending on the resistance from the sonicated medium. The fragmentation effect produced by ultrasonic energy depends on the energy amount that is released to the medium. However, only a portion of energy delivered is used in the production of aggregates and primary particles. Besides, an excess of energy may result in a re-agglomeration of fragmented clusters or physicochemical alterations on the material's surface (50).

## Lyophilization/Freeze Drying

Lyophilization also called freeze-drying, is a process involved in the removal of solvent (water) from sensitive products after being frozen. This process improves the stability without changing the product properties in such way, so the product can be easily preserved in long-term state and by adding water it can be easily reconstituted. The fundamental principle that governs this process is known as sublimation, a physical phenomenon that consists of a change of state from a solid-state to a vapor-state. Water sublimation occurs at pressures and temperatures below the triple point, that is, 4.579 mm Hg and 0.0099 °C. The lyophilization technique consists of three separate and interdependent processes:

### *Freezing*

Freezing is a crucial stage to establish the microstructures of the dry sample. For a complete solidification, the temperature must be low enough to freeze the sample. Since lyophilization is a change of state, the product must be pre-frozen correctly. The final temperature and the pre-freezing method can affect the ability to successfully lyophilize the sample. For example, small ice crystals suitable for preserving structures but difficult to lyophilize are the result of rapid freezing. While large ice crystals are the result of slow freezing.

The products are frozen depending on their eutectic point or glass transition point. The eutectic point is the one in which the solid, liquid and vapor phase coexist. The eutectic products are composed of substances that freeze at temperatures below to the solvent temperature (eutectic temperature). Therefore, before starting the process it is important to pre-freeze the products below the eutectic temperature. In contrast to the eutectic products, the suspension undergoes glass formation as its viscosity increase with temperature decrease. As a consequence, a vitreous solid is produced at the glass transition point.

### *Primary drying*

Once the product is pre-frozen, the optimal conditions are established to remove ice from the product by sublimation, which results in a dry and structurally intact product. This requires the control of the system parameters (temperature and pressure). Molecules usually migrate from the high pressure to low pressure. Considering that the vapor pressure and the temperature are correlated, it is important that the ice collector has a higher temperature than the product. Additionally, for optimum drying, lyophilization temperature must be equilibrated between the temperature at which the frozen product maintains its integrity and the temperature at which its vapor pressure is maximized.

### *Secondary drying*

Although a complete sublimation process has been carried out, the product still has a percentage of residual moisture, thus continuous drying is required to decrease the moisture to optimum values. This process is known as desorption since the low levels of water present in the product are desorbed. The desorption process is carried out at temperatures higher than the surrounding, but adaptable to the product sensitivity. Therefore, the storage temperature increase and the chamber pressure is minimized (51).

## Instrumentation

### Ultraviolet-Visible spectroscopy (UV-Vis)

Ultraviolet-visible (UV-Vis) spectroscopy is a quantitative analytical technique used in the primary characterization of the as-synthesized NPs. It is an efficient, simple, and applicable technique to different kinds of NPs. This technique is associated with the absorption of near-ultraviolet (180-390 nm) and visible (390-780 nm) radiation by chemical species. The near-ultraviolet and visible regions of the electromagnetic spectrum provide a precise amount of energy that results in electronic transitions from the highest occupied molecular orbital (HOMO) to the lowest unoccupied molecular orbital (LUMO). The energy difference between HOMO and LUMO is called the band gap. Each wavelength of light is associated to a particular energy. Therefore, a specific amount of energy delivered is capable to induce just one electronic transition, and the wavelength will be absorbed (52,53). The energy gap (54) could be estimated by the wavelength value corresponding to the intersection point using the following equations:

$$E_g = h \frac{c}{\lambda} \quad eV$$

$$E_g = \frac{1240}{\lambda} \quad eV$$

Where:

$E_g$ , Band-gap energy (eV)

$h$ , Planck's constant ( $6.626 \times 10^{-34} \text{ J} \cdot \text{s}$ )

$\lambda$ , Wavelength (nm)

$c$ , Speed of light ( $299792458 \times 10^{17} \text{ nm/s}$ )

$1 \text{ eV}$ ,  $1.6 \times 10^{-19} \text{ J}$

The greater the gap between energy levels, the greater the energy required, the shorter the wavelength. UV-Vis spectroscopy applies this concept to create the spectrum. On the devices, the output from the light source produces a beam focused to a prism that divides the incoming beam into its light beams of different wavelengths in the range from 200 to 800 nm. The light beam travels through the transparent cuvette which contains the liquid sample. Then, the detectors transform the incoming light into a current, with which the chart recorder creates a plot where a higher current means a greater intensity. The blank is a sample that contains everything except the analyte of interest, the solvent. The absorbance is calculated by the following equation:

$$A = \log_{10} \frac{I_0}{I}$$

The absorbance ( $A$ ) is a measure of the amount of light absorbed for each wavelength,  $I_0$  is the intensity of light from the reference cell (blank) and  $I$  is the intensity of light from the sample cuvette. The higher the value, the greater the absorbance of a particular wavelength. The Beer-Lambert Law states the absorbance is proportional to the concentration. Therefore, it is possible to measure the concentration of the sample in solution by a calibration graph. The Beer-Lambert Law is expressed by the following expression (53):

$$A = \epsilon * C * l$$

Where:

$A$ , Absorbance

$\epsilon$ , Molar absorptivity, constant for a particular substance at given wavelength ( $L \text{ mol}^{-1} \text{ cm}^{-1}$ )

$C$ , Concentration of the solution ( $\text{mol L}^{-1}$ )

$l$ , Dimension of the cuvette ( $\text{cm}$ )

### X-ray diffraction (XRD)

X-ray diffraction is a non-destructive analytical technique widely used for the identification of phases present in the crystal material (qualitative analysis), and the determination of their corresponding amounts (quantitative analysis), unit cell dimensions and crystallite sizes or preferential orientation. XRD technique is based on constructive interferences of scattered monochromatic X-rays and crystalline material (55). The geometrical interpretation of the XRD phenomenon has been well-established by W.L. Bragg. The geometrical conditions of diffraction and the determination of Bragg's law is detailed in Figure 6.

$$n\lambda = 2d\sin\theta$$

Where:

$n$ , Order of diffraction

$\lambda$ , Wavelength of the incident beam ( $nm$ )

$d$ , Distance between the crystal planes ( $nm$ )

$\theta$ , Angle of the diffracted beam ( $degree$ )

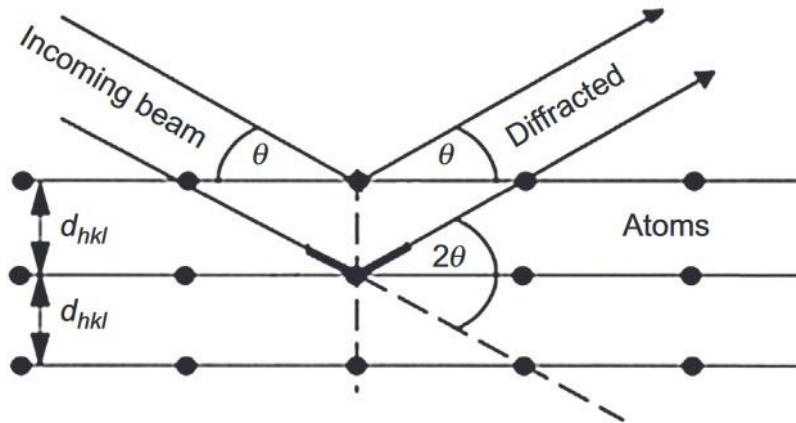


Figure 6: Schematic representation of geometrical conditions for diffraction. Retrieved from (56).

Bragg's equation is generally used to determine the distance between the planes of a crystalline structure. As well, it is possible to measure the angles at which constructive interference occurs. The result of the measurement is the so-called diffractogram. The diffraction pattern is a useful tool to identify crystalline structures and spatial groups of the present phases. Each phase produces a distinctive pattern that allows its identification. In some cases, multiple phases are identified in a system, the distinctive patterns of each phase overlap and the intensity of the diffraction peaks of the different phases are directly proportional to their amounts. The principal components of XRD diffractometers consist of three basic elements: X-ray tube, sample holder and X-ray detector. X-rays are generated inside the sealed tube by heating a filament to generate electrons. The as-generated electrons are accelerated in a high potential field and directed to a target material, which then emits X-rays. Once electrons have enough energy to displace the inner shell electrons of the target structure, characteristic X-ray patterns are generated (56,57).

## Transmission Electron Microscopy (TEM)

Electron microscope (EM) is a valuable instrument in the development of scientific theory and it contribute notably in nanotechnology and related areas. EMs were developed due to the magnification and resolution limitations of the traditional Light microscopes. The Transmission Electron Microscope (TEM) was the first type of EMs to be developed, following the same principle of their optical counterpart, except that TEM uses a focused electrons beam instead of light to observe and characterize the object on a nanometer ( $nm$ ) and micrometer ( $\mu m$ ) scales. TEM analysis provides information about the topography, morphology, chemical composition and crystallography of an object (58).

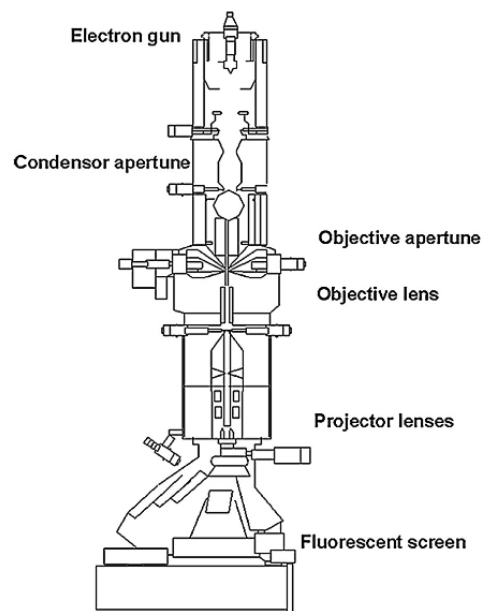


Figure 7: Schematic representation of a Transmission Electron Microscopy (TEM). Retrieved from (59).

The principle of operation of a TEM (Figure 7) is the electron scattering that is the base of image generation. The electron beam from the electron gun is focused into a small, thin beam by the use of the condenser lens, which restricts the size of the beam. The beam then hits the specimen and transmits parts of it depending on the specimen thickness. The objective lens focuses the transmitted parts into an image on a phosphor screen. The image that then passes through the intermediate and projector lens is fully enlarged. The screen detects the incoming image when the electrons hit it and light is generated, which allows to see the image. The dark-field of the image is a product of diffracted electrons while a light-field is produced by electrons scattered through the sample (59).



## Scanning Electron Microscopy (SEM)

Scanning electron microscopy has become a versatile advanced instrument for material characterization. SEM scans a focused electron beam over the solid specimen to create an image. The high-energy electrons of the beam interact with the surface of the material, generating several signals collected by detectors and used to get information about the surface topography, crystal structure, and orientation of the sample components. Areas ranging from 1  $\mu\text{m}$  - 5  $\mu\text{m}$  in thickness can be scanned using conventional SEM. The data are collected from a selected area of the surface, and a detailed 2D image is generated that exhibit the spatial variations in the properties.

The SEM instrument is based on the principle that the primary electrons generated by the electron gun are accelerated and hit the sample surface, interacting with the near-surface area to a certain depth in different ways. The primary electrons carry significant quantities of kinetic energy, which is dissipated inside the sample generating a variety of mixed signals by the electron interaction. These signals include secondary electrons (SE), backscattered and diffracted backscattered electrons, photons, visible light, and heat.

In the case of SEM, the two types of electrons used for imaging samples are secondary and backscattered electrons. Secondary electrons that are a result of inelastic interactions between the incoming electron beam and the specimen display the morphology and topography of samples. Unlike the secondary electrons, the backscattered electrons, reflected after the stable interactions between the beam and the specimen, exhibit the contrasts for the rapid phase discrimination. Photons or characteristic X-rays are produced for each element present in the mineral after its excitation, by the beam (60–62).

Energy-dispersive X-ray spectroscopy (EDS or EDX) is involved in the identification of the elemental composition of a sample by using scanning electron microscope. The elemental microanalysis is determined by the characteristic X-rays emitted from a specimen being examined. The elemental analysis is achieved in a spot mode in which the beam is localized on an area of interest within the field of view, the so-called *point analysis*, and the specific X-ray intensity is measured. The intensity of the characteristic X-ray peaks recognized in the EDS spectrum is not a quantitative measure of the element concentration, although relative quantities can be estimated from relative peak heights (63,64).

# Chapter 3

## Results & Discussion

### Experimental procedure

#### Materials

For the preparation of silver selenide colloidal nanoparticles, selenous acid,  $\text{H}_2\text{SeO}_3$  (99%, Sigma-Aldrich), and silver nitrate,  $\text{AgNO}_3$  (99%, EMSURE), were the precursors, D(+) fructose from Sigma-Aldrich was the reducing agent, soluble corn starch from Sigma-Aldrich was the stabilizing agent, and distilled water was the solvent. All chemicals were used without any additional chemical purification.

#### Green synthesis of silver selenide NPs

The green synthesis of  $\text{Ag}_2\text{Se}$  NPs, was carried out by a facile co-precipitation method. Selenous acid (0.44 g) and  $\text{AgNO}_3$  (1.73 g) were separately dissolved in deionized water at room temperature.

The preparation of  $\text{Ag}_2\text{Se}$  NPs and the associated control experiments are described in Table 2. For  $\text{Ag}_2\text{Se}$  NPs preparation, 5 mL of 1.7 mM  $\text{H}_2\text{SeO}_3$  and 10 mL of 3.4 mM  $\text{AgNO}_3$  were added into a 300 mL glass beaker with a ratio of 1:2. Immediately, starch and fructose at different concentrations was added to the reaction mixture and ultrasound irradiation was carried out with ultrasonic processors (DAIGGER GE 505, 500 W, 20 kHz) immersed directly into the reaction solution (Figure 8). The operating condition was 59-s pulse on and 5-s pulse off time with amplitude of 70% for 30 min. The formation of  $\text{Ag}_2\text{Se}$  NPs was confirmed by the appearance of brown solution with the lapse of time.

Table 2: Reaction parameters for the production of  $\text{Ag}_2\text{Se}$  NPs. The total reaction volume 100 mL.

N°	COMPOSITION	V(DW) mL	S mg mL <sup>-1</sup>	F mg mL <sup>-1</sup>	V(Ag <sup>+</sup> ) mL	V(Se <sup>4+</sup> ) mL	TIME min
E <sub>1-1</sub>	$\text{AgNO}_3 + \text{H}_2\text{SeO}_3 + \text{F} + \text{S}$	85	10	5	10	5	30
E <sub>1-2</sub>	$\text{AgNO}_3 + \text{H}_2\text{SeO}_3 + \text{F} + \text{S}$	85	10	10	10	5	30
E <sub>1-3</sub>	$\text{AgNO}_3 + \text{H}_2\text{SeO}_3 + \text{F} + \text{S}$	85	10	20	10	5	30
E <sub>1-4</sub>	$\text{AgNO}_3 + \text{H}_2\text{SeO}_3 + \text{F} + \text{S}$	85	10	40	10	5	30
C <sub>1-1</sub>	$\text{AgNO}_3 + \text{H}_2\text{SeO}_3 + \text{F}$	85	10	0	10	5	30
C <sub>1-2</sub>	$\text{AgNO}_3 + \text{H}_2\text{SeO}_3 + \text{S}$	85	0	10	10	5	30
C <sub>1-3</sub>	$\text{AgNO}_3 + \text{H}_2\text{SeO}_3$	85	0	0	10	5	30

V: volume; DW: distilled water; F: fructose; S: Starch; E: experiment; C: control.

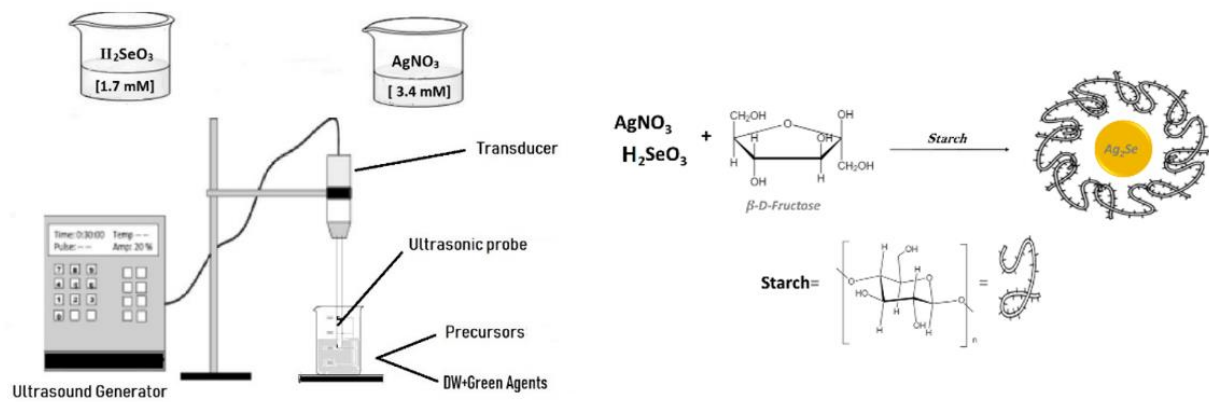
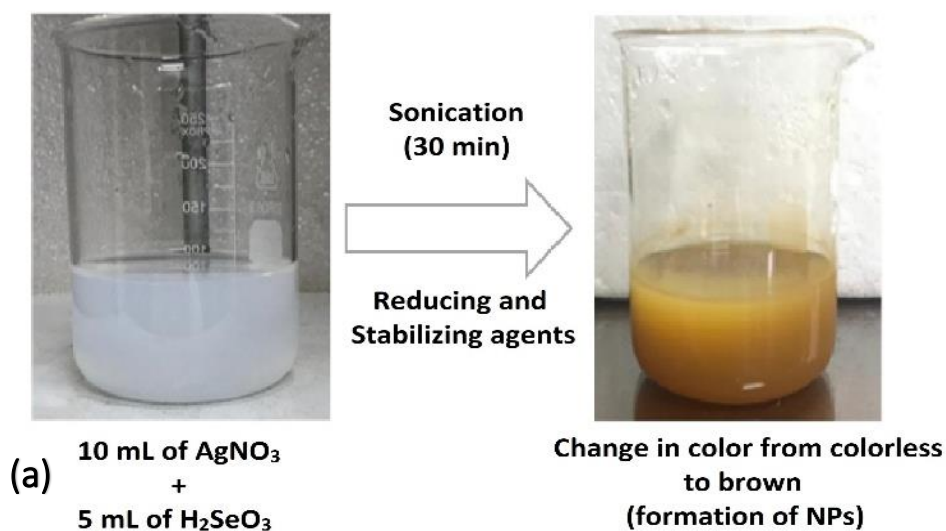


Figure 8: Schematic diagram showing the method of synthesis of Ag<sub>2</sub>Se NPs. Adapted from reference (65).

## Instrumentation

### Visual results of Ag<sub>2</sub>Se NPs

The initial prediction of the formation of Ag<sub>2</sub>Se NPs is the visual color change of the samples after sonication. It clearly shows that the starting colorless reaction mixture becomes brown under sonication in the presence of fructose and starch as reducing and stabilizing agents, respectively (Figure 9a). For comparison purposes, an aqueous solution of 10 mL of AgNO<sub>3</sub> and 5 mL of H<sub>2</sub>SeO<sub>3</sub>, was exposed to ultrasound energy, used as a control (Figure 9b). No change in color in this solution was observed, confirming also the effectiveness of fructose and starch as green agents that promote the production of Ag<sub>2</sub>Se NPs.



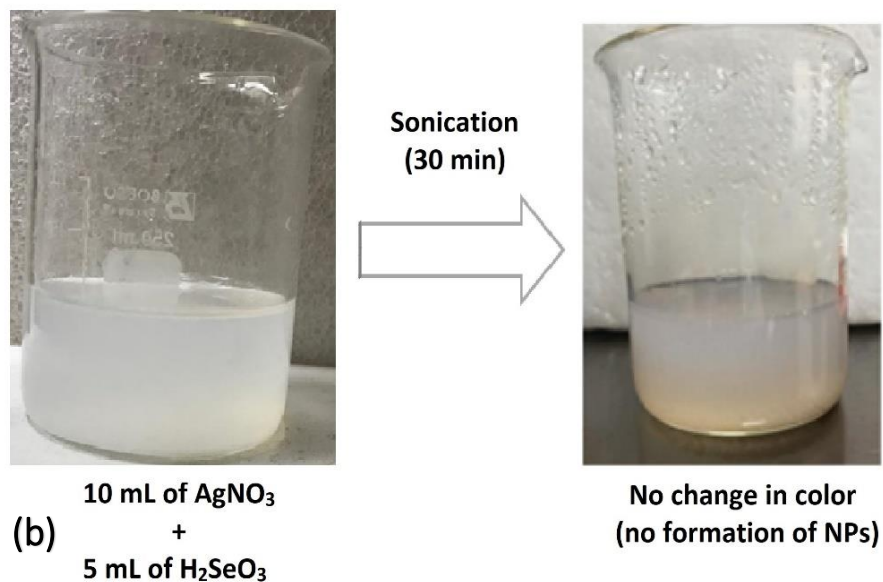


Figure 9: Pathway for the synthesis of Silver selenide NPs (a) sample E1-4 and (b) control reaction.

As the fructose concentration increases from  $10 \text{ mg mL}^{-1}$  to  $40 \text{ mg mL}^{-1}$ , a greater color intensity of the samples is observed (Figure 10a). Therefore, it is estimated that the production of nanoparticles would be higher with the maximum fructose concentration. In addition, no sample shows precipitation. On the other hand, as shown in Figure 10b, control samples without fructose do not show a color change after being subjected to ultrasonic irradiation, unlike the control sample  $C_{1-1}$  with  $40 \text{ mg mL}^{-1}$  of fructose that has an orange color due to the formation of nanoparticles.

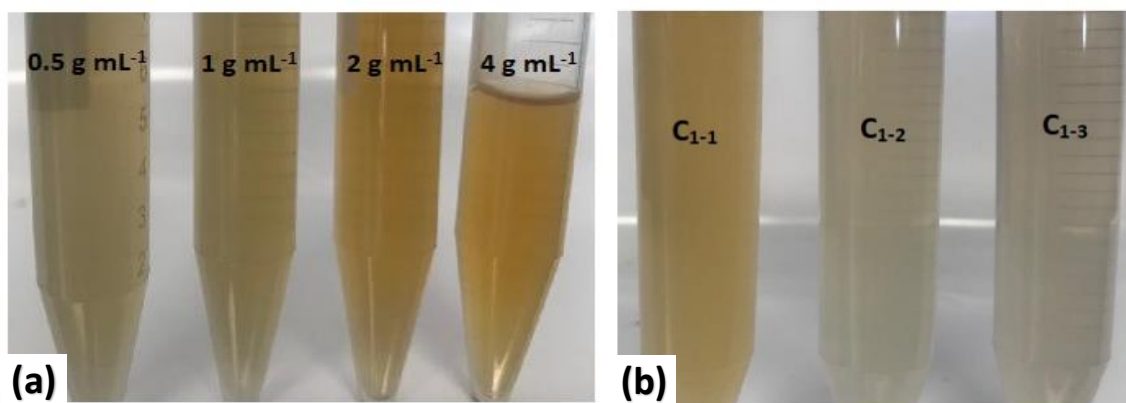


Figure 10: Color pattern of silver selenide nanoparticles under 30 min of ultrasound irradiation (a) different fructose concentration and (b) control experiments.

## UV-Vis study of Ag<sub>2</sub>Se NPs

UV-Vis spectrometry is one of the most useful technique to ascertain the formation and stability of nanoparticles, in aqueous solution in the present case. In order to study the size distribution and colloidal stability of Ag<sub>2</sub>Se nanoparticles, UV-Vis spectra were recorded using a LAMBDA 1050 UV-Vis Spectrophotometer (175 to 3300 nm), PerkinElmer®. The samples were placed in a quartz cuvette for analysis whereas distilled water was used as a reference solvent.

The formation of Ag<sub>2</sub>Se NPs was confirmed by the appearance of the absorbance band and wavelength position in the visible region at 385 nm - 446 nm, similar to those reported in literature (2,66) (Figure 11a). In this range, single absorption peak give information of shape, size and size distribution represents the characteristic absorbance band of spherical and aggregated NPs (67,68).

In order to confirm the role of fructose in the reduction process, if we increase the fructose concentration, there is increase in wavelength up to 413 nm as shown in Figure 11a. The same experiment was carried out in absence of fructose. The corresponding UV-Vis absorption spectra is shows in Figure 11b. The highest intensity absorbance of Ag<sub>2</sub>Se NPs was observed at 40 mg mL<sup>-1</sup> fructose concentration, whereas below 10 mg mL<sup>-1</sup> the formation of the absorption band was not observed, therefore there was no reaction and no nanoparticles were synthesized. The intensity and wavelength were changed when the fructose concentration is low or high, due to either the insufficient presence of reducing agent or the formation of clusters. The variations in the intensity of absorption values signify changes in the particle size (69).

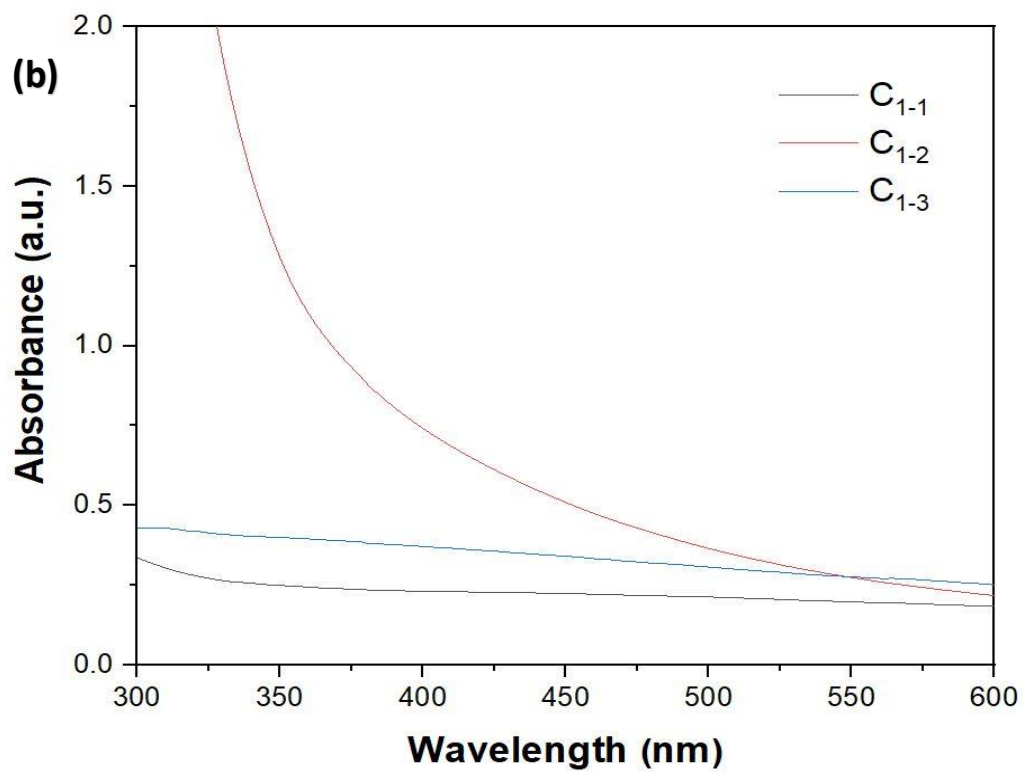
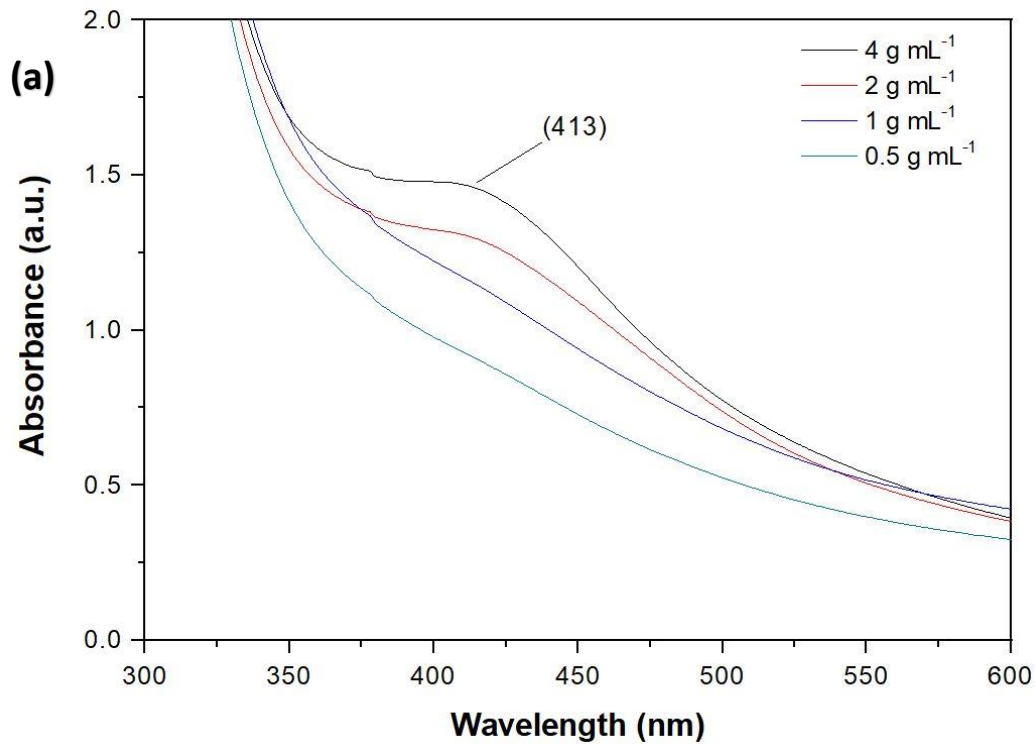


Figure 11: UV-Vis spectrum of as-synthesized  $\text{Ag}_2\text{Se}$  NPs (a) different fructose concentration, (b) control experiments detailed in Table 1.1.

After confirm the production of NPs and the efficiency of fructose in the reaction, the stability of Ag<sub>2</sub>Se NPs stored at room temperature was monitored. The UV-Vis spectrums were recorded for 15, 30, and 60 days (Figure 12). It is observed that post 15 days there is a slight increase in the intensity of the absorption band that may due to a change in the nanoparticles concentration or cluster formation. After 30 and 60 days, there is a minimal increase in the absorption band intensity that confirms the stability of Ag<sub>2</sub>Se NPs for a long period of time.

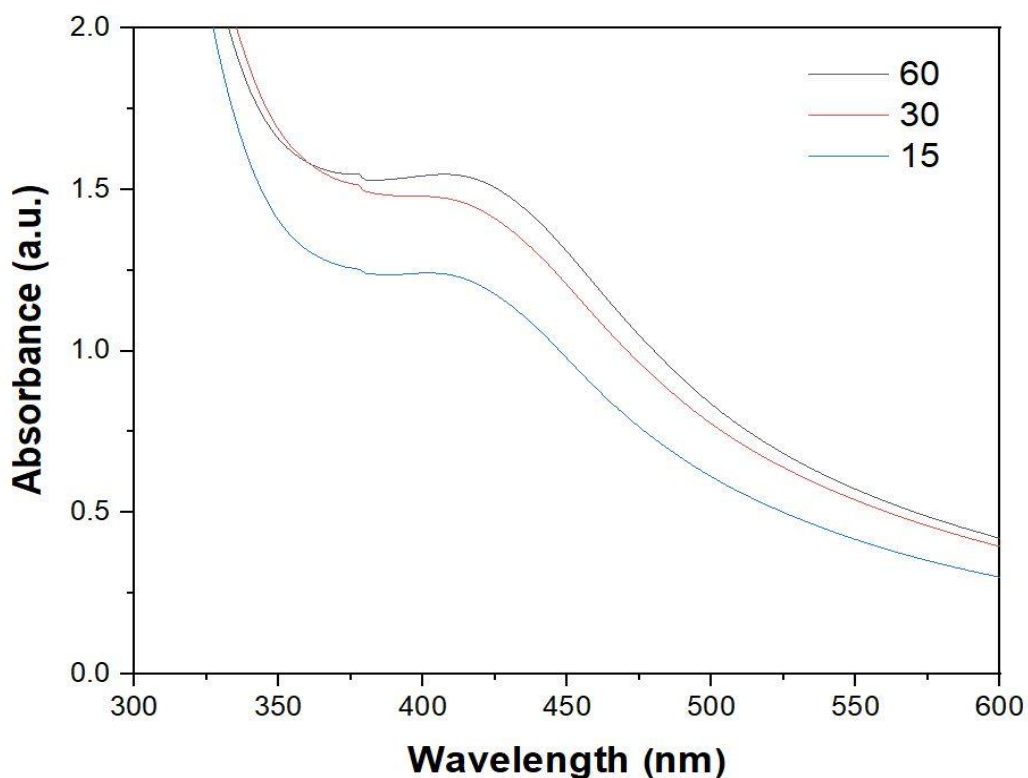


Figure 12: UV-Vis spectrum of Ag<sub>2</sub>Se NPs under sonication for 30 min and stored at room temperature for 15, 30, and 60 days.

## XRD

X-ray diffraction (XRD) analysis on thin films of Ag<sub>2</sub>Se NPs was carried out to identify the phase structure and determine the crystallite size using PANanalytical brand  $\Theta - 2\Theta$  configuration (generator-detector) X-ray tube, copper at  $\lambda = 1.54059 \text{ \AA}$  and EMPYREAN diffractometer.

The XRD patterns of silver selenide NPs under ultrasound energy are showed in Figure 3.6. Ag<sub>2</sub>Se NPS can exist as either orthorhombic and cubic phase. According to Kumashiro et al. (70) all samples during the cooling process, undergo an  $\alpha \rightarrow \beta$  phase transition. As Ag<sub>2</sub>Se is

a non-stoichiometric compound in both phases can exist dissolved silver atoms with  $\text{Ag}_2\text{Se}$  as a single phase. In addition, they mention that the silver solubility is higher in the  $\alpha$ -phase than the  $\beta$ -phase (70). Therefore, excess of Ag will be dissociated in AgNPs and/or segregation of metallic silver. As shown in Figure 13, the characteristic diffraction peak observed at  $2\theta = 36.1^\circ, 44.1^\circ, 52.3^\circ, 64.5^\circ$  correspond to (002), (112), (022), (222) planes which conform the cubic phase  $\alpha\text{-Ag}_2\text{Se}$  (JCPDS, 98-003-3627). The additional diffraction patterns observed at  $2\theta = 25.8^\circ, 31.8^\circ, 33.3^\circ, 34.8^\circ, 39.5^\circ, 40.1^\circ, 43.5^\circ, 46.6^\circ, 50.9^\circ, 54.6^\circ$  correspond to (012), (102), (112), (121), (031), (122), (210), (004), (221), (222) planes which can be indexed to orthorhombic phase  $\beta\text{-Ag}_2\text{Se}$  with the naumannite structure conforming  $\text{P2}_1\text{2}_1\text{2}_1$  (19) space group (JCPDS, 98-001-5213). The prominent peak at  $2\theta = 37.6^\circ$  corresponding to (111) plane suggest the presence of elemental silver, as well as, short peaks from selenium that was reduced to their elemental form in the final sample.

The presence of both orthorhombic- and cubic-phase of silver selenide is due to the acoustic cavitation phenomenon which causes the formation of vapor bubbles that after collapses producing localized hot spots with temperatures up to 5000 K, high pressure (<20 MPa), and very high cooling rates (71). In other words, this method offers optimal conditions for the formation of both phases at the same time. Furthermore, some diffraction peaks present widening by the overlapping phases mainly due to the small particle size show confirmed by TEM micrographs (Figure 14).

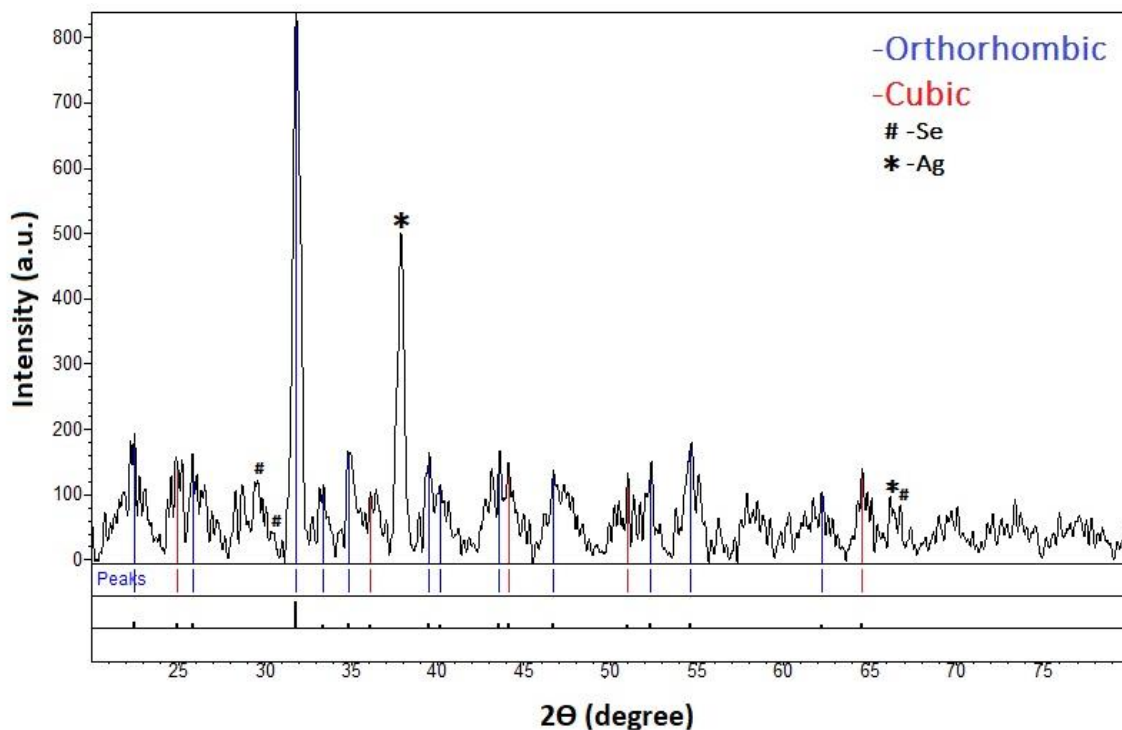


Figure 13: XRD diffractogram of  $E_{1-3}$  sample. The red and blue vertical lines correspond to the cubic and orthorhombic phases of  $\text{Ag}_2\text{Se}$ , respectively.



## Crystalline size

In order to obtain information about the crystallite size, the broadening of diffraction peak in the XRD is related with the particle size by Debye-Scherrer equation (72):

$$L = \frac{K\lambda}{B \cos \Theta}$$

Where,

$\lambda$ , X-ray wavelength (0.154059nm)

$B$ , The line broadening at half maximum (FWHM)

$K$ , Constant related to crystalline shape = 0.93

$L$ , Linear dimension of the particle

For this estimation, the most intense diffraction peak at  $2\Theta = 31.8^\circ$  corresponding to (102) crystallographic plane was used. FWHM ( $2\Theta$ ) = 0.310, the wavelength of X-rays ( $\lambda$ ) is 0,154059 nm. Taken into account that the values of FWHM and peak position ( $2\Theta$ ) must be in radians, the crystallite size:

$$L = \frac{0.93 * 0.154059}{5.4 \times 10^{-3} * \cos(0.55)}$$

$$L = 26.5 \text{ nm}$$

The crystallite size obtained through the Scherrer formula is related with the TEM micrographs where the range of the average particle size is between 11.26 to 27.55 nm. This result is consistent with the particle size already reported (71,73) .

## TEM

The most straightforward way to establish the size, shape and morphologies of produced nanoparticles was using Transmission Electron Microscopy, TEM (FEI, TECNAI, G2spirit twin, Holland).

TEM micrographs at 200 nm and 500 nm scale were subjected to particle size distribution through the use of ImageJ software. This software generates a .CSV files with information about the area of the as-synthesized nanoparticles. Ag<sub>2</sub>Se NPs are round-shaped. Therefore, the diameter is calculated from the area formula of a circle.

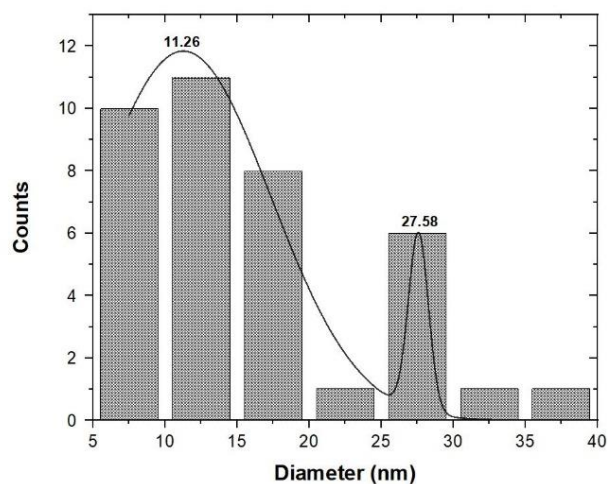
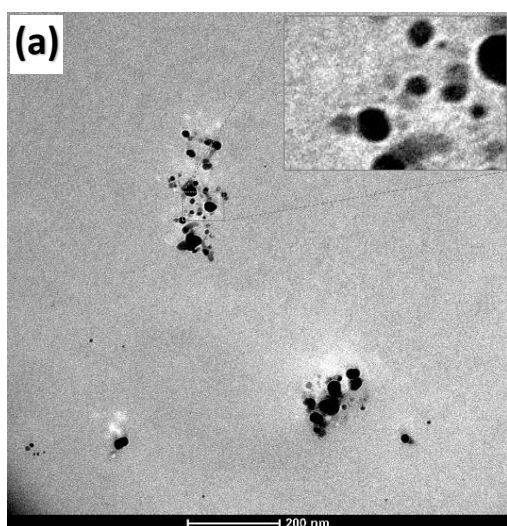
$$A = \pi r^2$$

The diameter is calculated using the relationship:  $d = 2 * r$ . Then, through the use of OriginPro software, a histogram with the diameter data is generated, which is fitted with Gaussian function to determine the average size of the NPs.

Table 3: Particle size distribution of Ag<sub>2</sub>Se NPs analyzed in figure 6. For each micrograph is detailed the average size, total counts, and the range of size at which the largest number of nanoparticles belong.

Figure 6	Average size (nm)	Total Counts	Range of size
(a)	11.26 - 27.58	38	[5 – 30 nm] 78%
(b)	17.49 – 27.55	27	[10 – 40 nm] 51%

The results obtained from TEM images show that the as-synthesized Ag<sub>2</sub>Se NPs are round in shape with a broad size distribution. The corresponding size distribution for the E<sub>1-3</sub> sample is 7-27 nm as displayed in Figure 14 (a) and (b).



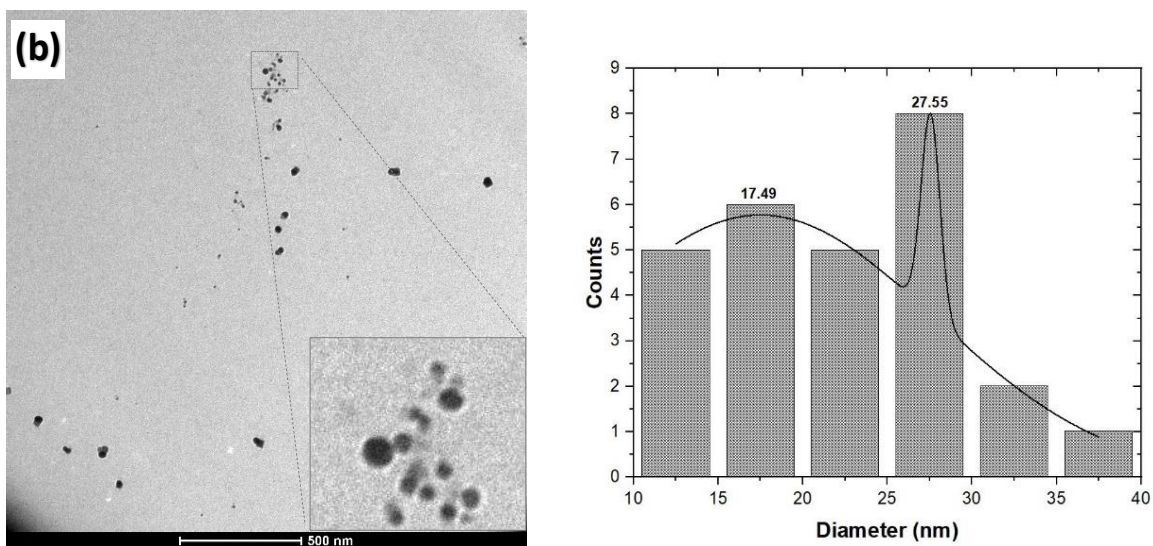


Figure 14: TEM micrographs of  $Ag_2Se$  NPs in colloidal solution. The first column is the TEM images at different magnification where the NPs are the black spots. The second column contains the histograms plots with the average sizes values of silver selenide NPs.

In the presence of starch only (sample preparation  $C_{1-2}$ ), the micrographs (Figure 15 (a) and (b)) show that the synthesized particles morphology changes from spherical to cubic and rod shaped nanocrystals with a large particle size, as compared to Figure 14. It is clear that large aggregate nanostructures were formed in the absence of fructose as a reducing agent. It might be attributed to the fact that starch is a natural polysaccharide that can be decomposed in amylose and amylopectin, natural polymers formed by long chains of  $\alpha$ -D-glucose molecules.  $\alpha$ -D-glucose, similar to D-fructose, is a natural sugar that acts as a reducing agent in the production of nanoparticles (74). Therefore, the starch, after its possible degradation, might have acted as the reducing agent instead of solely the stabilizing agent. As a consequence, aggregated cubic and rod nanoparticles of different sizes were formed, since there is little to no stabilizing matrix that controls the NP features (size, shape, stability). These results confirm the role of fructose as a strong reducing sugar and the starch as a stabilizing matrix in the production of nanoparticles with optical and structural controllable properties.

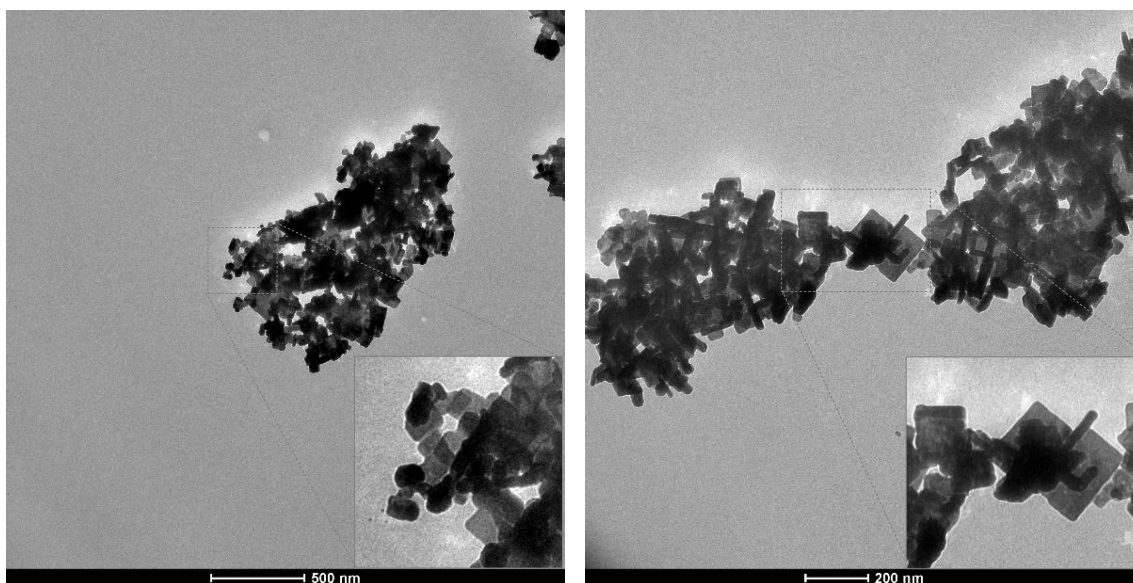


Figure 15: TEM images of  $\text{Ag}_2\text{SeNPs}$  prepared in absence of reducing agent.

#### SEM – EDS

The elemental analysis/mapping of  $\text{Ag}_2\text{Se}$  NPs were performed non-destructively using SEM (TESCAN, MIRA 3) equipped with energy-dispersive X-ray spectrometry EDS (Bruker Nano GmbH, Quantax). The samples were prepared by casting one drop of the NP solution on a carbon coated copper grid and drying at room temperature.

The energy dispersive X-ray spectrometry (EDS) technique was employed to study the chemical composition and purity of  $\text{Ag}_2\text{Se}$  material. The EDS spectrum, taken from a selected area of SEM image, shows prominent elemental peaks related to silver, selenium, carbon and oxygen in the as-synthesized  $\text{Ag}_2\text{Se}$  NPs (Figure 16). The C and O detected in the spectrum that arise from mainly the stabilizing agent (starch) and residual reducing agent (fructose). The identification line for the major emission energy of selenium is observed in the range of 1.2 - 1.6 keV while the one of silver is observed in the range of 2.6 - 4 keV. These observed peaks of selenium and silver, due to their presence in  $\text{Ag}_2\text{Se}$  NPs, corroborate elemental peaks reported in literature (2,75). Therefore, the EDS spectrum confirms the presence of silver and selenium atoms in the as-synthesized  $\text{Ag}_2\text{Se}$  NPs. Moreover, silver and selenium are in 2:1 proportion, which suggests the chemical formula  $\text{Ag}_2\text{Se}$ .

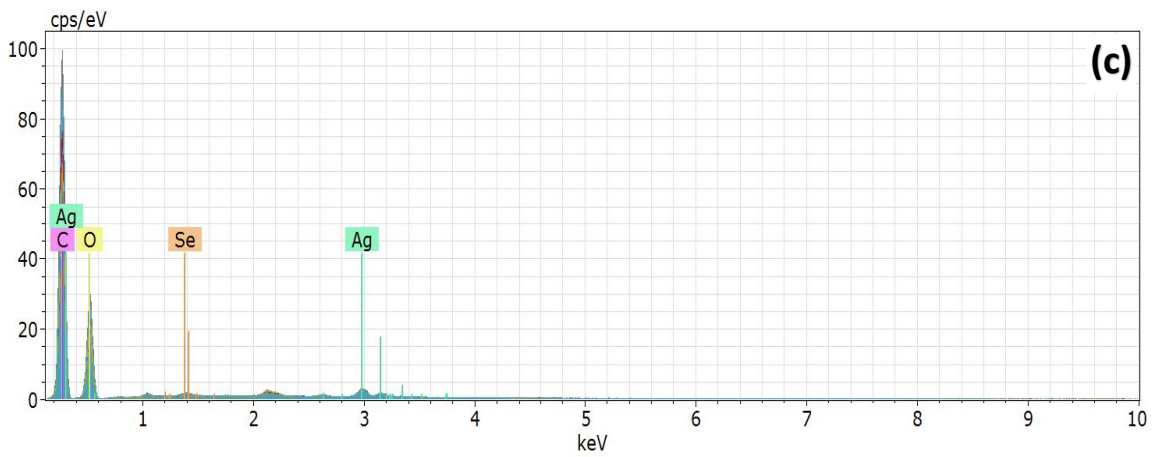
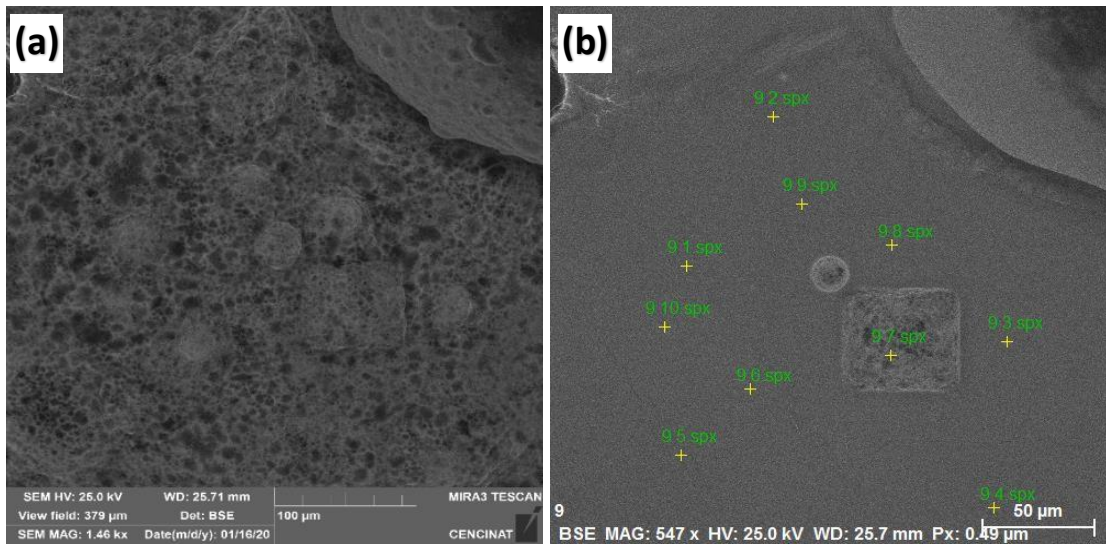


Figure 16: (a) SEM image; (b) figure gives a selected area for EDS measure and elemental analysis; (c) EDS spectrum of  $\text{Ag}_2\text{Se}$  nanoparticles.

# Chapter 4

## Conclusions & Outlook

### Conclusions

The aqueous green synthesis of silver selenide nanoparticles described in Chapter 3 was successful as it demonstrated the efficiency of fructose and starch as reducing and stabilizing natural agents, respectively, in the presence of silver and selenium precursors. Among the different sources of selenium, selenous acid ( $\text{H}_2\text{SeO}_3$ ), sodium selenite ( $\text{Na}_2\text{SeO}_3$ ), and selenium tetrachloride ( $\text{SeCl}_4$ ), only the first one gave rise to the desired nanomaterials. Similarly, different natural sugars like glucose, fructose and sucrose were screened with different concentrations of starch for their ability to promote the synthesis of  $\text{Ag}_2\text{Se}$  NPs. In this regard, the best results were obtained with selenous acid.

The easiest evidence of the formation of  $\text{Ag}_2\text{Se}$  NPs was the visual color change of the samples under ultrasound irradiation in the presence of both starch and fructose. In order to confirm the presence of as-prepared NPs, the UV-Vis spectra show the absorbance band and wavelength position in the visible region in the range of 385-446 nm. The highest intensity absorbance was observed at the maximum fructose concentration ( $40 \text{ mg mL}^{-1}$ ), whereas, below  $10 \text{ mg mL}^{-1}$ , no formation occurred. The XRD patterns show the presence of both orthorhombic and cubic phases of silver selenide, as well as, some prominent peaks that suggest the presence of elemental silver and elemental selenium in the final sample. The widening of the major peaks is attributed to the overlapping phased mainly due to the small size of the NPs that was determined using the Scherrer equation. The crystallite size is comparable to the NP size that was determined from TEM micrographs displaying NPs ranging from 11.26 to 27.55 nm. Moreover, TEM images confirm the production of uniform, monodispersed and spherical  $\text{Ag}_2\text{Se}$  NPs only in the presence of both natural agents, fructose and starch.

On the other hand, the elemental analysis performed using SEM-EDS technique corroborated the previous results. In addition to C and O peaks due mainly to starch, the EDS spectrum showed the prominent elemental peaks related to silver and selenium atoms in a 2:1 ratio confirming, once again, the obtained of  $\text{Ag}_2\text{Se}$  NPs.

## **Outlook**

To corroborate once more the results obtained previously, X-rays photoelectron spectroscopy analysis should be carried out in order to estimate the stoichiometry, chemical state, and electronic structure of the elements present in the as-synthesized silver selenide NPs. Moreover, mechanistic aspects that explain the formation of these stable NPs should be explored. Additionally, biological tests should be performed on Gram (+) and Gram (-) bacteria in order to prove the antibacterial properties of Ag<sub>2</sub>Se nanoparticles.

On the other hand, the methodology should be optimized based on new reaction parameters: other Se and Ag precursors along with other sugars should be screened. On the other hand, one may think to increasing the reaction time while constantly stirring to work under homogenous solution and same temperature.

## Bibliography

1. Fulekar M. Nanotechnology: Importance and applications [Internet]. Nanotechnology: Importance and applications. Nwe Delhi: I.K. International Publishing House Pvt. Ltd.; 2010 [cited 2020 Jan 25]. 173 p. Available from: <https://books.google.com.ec/books?hl=es&lr=&id=wYie57y1zj8C&oi=fnd&pg=PR7&dq=nanoscience+and+nanotechnology+importance&ots=knXFzI5dDY&sig=1VsPvagQOLWWqMXENLC28t9KiCo#v=onepage&q=nanoscience and nanotechnology importance&f=false>
2. Sibiya PN, Moloto MJ. EFFECT OF PRECURSOR CONCENTRATION AND pH ON THE SHAPE AND SIZE OF STARCH CAPPED SILVER SELENIDE (Ag<sub>2</sub>Se) NANOPARTICLES. Vol. 11, Chalcogenide Letters. 2014.
3. Abdullayev AG, Shafizade RB, Krupnikov ES, Kiriluk K V. Phase formation and kinetics of the phase transition in Ag<sub>2</sub>Se thin films. Thin Solid Films. 1983 Aug 19;106(3):175–84.
4. Kharissova O V., Dias HVR, Kharisov BI, Pérez BO, Pérez VMJ. The greener synthesis of nanoparticles. Trends Biotechnol. 2013;31(4):240–8.
5. Fraile MC. Estudio de las interacciones entre nanopartículas de metales nobles y ADN. 2016;39. Available from: <https://idus.us.es/xmlui/bitstream/handle/11441/50465/Fraile Romero%2C María Concepción.pdf?sequence=1&isAllowed=y>
6. Castro-Guerrero CF, Morales-Cepeda AB, Hernández-Vega LK, Díaz-Guillén MR. Fructose-mediated gold nanoparticles synthesis. Cogent Chem [Internet]. 2018;4(1):1–7. Available from: <http://doi.org/10.1080/23312009.2018.1447262>
7. Raveendran P, Fu J, Wallen SL, Hill C, Carolina N. Completely “Green” Synthesis and Stabilization of Metal Nanoparticles. Rev la Soc Química del Perú. 2003;125:13940–1.
8. Sotelo E. Departamento de Química Física y Analítica. Universidad de Oviedo; 2013.
9. ISO/TS 80004-12:2016(en), Nanotechnologies — Vocabulary — Part 12: Quantum phenomena in nanotechnology [Internet]. [cited 2019 Dec 23]. Available from: <https://www.iso.org/obp/ui/#iso:std:iso:ts:80004:-12:ed-1:v1:en>
10. The Royal Society, Engineering TRA of, Dowling a, Clift R, Grobert N, Hutton D, et al. Nanoscience and nanotechnologies: opportunities and uncertainties. London R Soc R Acad Eng Rep [Internet]. 2004;46(July):618–618. Available from: <http://scholar.google.com/scholar?hl=en&btnG=Search&q=intitle:Nanoscience+and+nanotechnologies+:+opportunities+and+uncertainties#0>
11. Pitkethly MJ. Nanomaterials - The driving force. Mater Today. 2004;7(12)



SUPPL.):20–9.

12. Poole CP, Frank Owens JJ. INTRODUCTION TO NANOTECHNOLOGY Library of Congress Cataloging-in-Publication Data. Available from: <https://startinnovationblog.files.wordpress.com/2015/12/nanotechnology-by-charlespoole.pdf>
13. Leson A. There is plenty of room at the bottom. *Vak Forsch und Prax.* 2005;17(3):123.
14. Fanfair D, Desai S, Kelty C. The Early History of Nanotechnology \* [Internet]. [cited 2019 Oct 22]. Available from: <http://frazer.rice.edu/nanotech>
15. Hulla JE, Sahu SC, Hayes AW. Nanotechnology: History and future. *Hum Exp Toxicol* [Internet]. 2015;34(12):1318–21. Available from: <https://journals.sagepub.com/doi/pdf/10.1177/0960327115603588>
16. Suresh S. Semiconductor Nanomaterials, Methods and Applications: A Review. *Nanosci Nanotechnol.* 2013;3(3):62–74.
17. Xu J, Wang G, Li S, Shao W, Zhang X. The influence of particle shape on magnetoresistance effect of two-dimensional metal-semiconductor composites. *J Appl Phys.* 2013;114(12).
18. Stetsyk NV, Antonyuk V., Rudka M. Semiconductor Nanomaterials and Nanocrystals. *J NANO- Electron Phys.* 2015;7(2):1–12.
19. Helan PPJ, Mohanraj K, Sivakumar G. Synthesis and characterization of  $\beta$ -Ag<sub>2</sub>Se and  $\beta$ -AgCuSe nanoparticles via facile precipitation route. *Trans Nonferrous Met Soc China (English Ed.* 2015 Jul 1;25(7):2241–6.
20. Shimojo F, Okazaki H. Boundary Condition Effect in MD Simulation: A Case of the  $\alpha \rightarrow \beta$  Phase Transition in Superionic Conductor Ag<sub>2</sub>Se. *J Phys Soc Japan.* 1993;62(1):179–82.
21. Ferhat M, Nagao J. Thermoelectric and transport properties of  $\beta$ -Ag<sub>2</sub>Se compounds. *J Appl Phys.* 2000 Jul 15;88(2):813–6.
22. Cao H, Xiao Y, Lu Y, Yin J, Li B, Wu S, et al. Ag<sub>2</sub>Se complex nanostructures with photocatalytic activity and superhydrophobicity. *Nano Res.* 2010;3(12):863–73.
23. Materials Project. mp-568889: Ag<sub>2</sub>Se (orthorhombic, P222<sub>1</sub>, 17) [Internet]. [cited 2020 Jan 22]. Available from: <https://materialsproject.org/materials/mp-568889/>
24. Iqbal P, Preece JA, Mendes PM. Nanotechnology: The “Top-Down” and “Bottom-Up” Approaches. In: *Supramolecular Chemistry.* John Wiley & Sons, Ltd; 2012.
25. Biswas A, Bayer IS, Biris AS, Wang T, Dervishi E, Faupel F. Advances in top-down and bottom-up surface nanofabrication: Techniques, applications & future prospects.

Vol. 170, *Advances in Colloid and Interface Science*. 2012. p. 2–27.

26. Tseng AA. *Nanofabrication: Fundamentals and applications*. Nanofabrication: Fundamentals and Applications. World Scientific Publishing Co.; 2008. 1–574 p.
27. Anastas P, Eghbali N. *Green chemistry: Principles and practice*. *Chem Soc Rev*. 2010;39(1):301–12.
28. Iravani S, Korbekandi H, Mirmohammadi S V., Zolfaghari B. Synthesis of silver nanoparticles: Chemical, physical and biological methods. Vol. 9, *Research in Pharmaceutical Sciences*. Isfahan University of Medical Sciences(IUMS); 2014. p. 385–406.
29. Kaler A, Pater N, Chand Banerjee U. *Green Synthesis of Silver Nanoparticles*. 2010.
30. Abid JP, Wark AW, Brevet PF, Girault HH. Preparation of silver nanoparticles in solution from a silver salt by laser irradiation. *Chem Commun*. 2002;7:792–3.
31. Henam SD, Ahmad F, Shah MA, Parveen S, Wani AH. Microwave synthesis of nanoparticles and their antifungal activities. *Spectrochim Acta - Part A Mol Biomol Spectrosc* [Internet]. 2019;213:337–41. Available from: <https://doi.org/10.1016/j.saa.2019.01.071>
32. Zanella R. Metodologías para la síntesis de nanopartículas controlando forma y tamaño. *Mundo Nano Rev Interdiscip en Nanociencia y Nanotecnología*. 2014;5(1):69–81.
33. Zhu J, Koltypin Y, Gedanken A. General sonochemical method for the preparation of nanophasic selenides: Synthesis of ZnSe nanoparticles. *Chem Mater*. 2000;12(1):73–8.
34. Korbekandi H, Iravani S. Silver Nanoparticles. In: *The Delivery of Nanoparticles* [Internet]. InTech; 2012 [cited 2019 Oct 22]. Available from: <http://www.intechopen.com/books/the-delivery-of-nanoparticles/silver-nanoparticles>
35. Suvorova AI, Tyukova IS, Trufanova EI. Biodegradable starch-based polymeric materials. *Russ Chem Rev*. 2000;69(5):451–9.
36. Buléon A, Colonna P, Planchot V, Ball S. Starch granules: Structure and biosynthesis. *Int J Biol Macromol*. 1998;23(2):85–112.
37. Van Soest JGG, Vliegthart JFG. Crystallinity in starch plastics: Consequences for material properties. *Trends Biotechnol*. 1997;15(6):208–13.
38. Yu H, Cheng L, Yin J, Yan S, Liu K, Zhang F, et al. Structure and physicochemical properties of starches in lotus (*Nelumbo nucifera* Gaertn.) rhizome. *Food Sci Nutr*. 2013;1(4):273–83.

39. Rodriguez P, Muñoz-Aguirre N, San-Martín Martínez E, González de la Cruz G, Tomas SA, Zelaya Angel O. Synthesis and spectral properties of starch capped CdS nanoparticles in aqueous solution. *J Cryst Growth*. 2008;310(1):160–4.
40. Lu DR, Xiao CM, Xu SJ. Starch-based completely biodegradable polymer materials. *Express Polym Lett*. 2009;3(6):366–75.
41. Engelking LR, Engelking LR. Chapter 18 – Carbohydrate Structure. *Textb Vet Physiol Chem*. 2015;118–23.
42. Cole L, Kramer PR, Cole L, Kramer PR. Chapter 5.1 – Macronutrients. *Hum Physiol Biochem Basic Med*. 2016;157–64.
43. Detz RJ, Reek JNH, Van Der Zwaan BCC. The future of solar fuels: When could they become competitive? *Energy Environ Sci*. 2018;11(7):1653–69.
44. Huynh WU, Dittmer JJ, Alivisatos AP. Hybrid nanorod-polymer solar cells. *Science* (80- ). 2002;295(5564):2425–7.
45. Hpperk U, Setlur A, Collins J, Aguilar Z. Luminescence and Display Materials [Internet]. [cited 2019 Oct 22]. Available from: [https://books.google.com.ec/books?id=ufDefc0Kb1QC&pg=PA16&lpg=PA16&dq=H.+Mattoussiet++al.,J.++Appl.++Phys.83,+7965+\(1998\).&source=bl&ots=mzikSAFwhU&sig=ACfU3U2zKfMq7M0bIOy-VwDqYQxmND\\_WSw&hl=es&sa=X&ved=2ahUKEwikrd239ZrIAhWpmOAKHQ-ICxgQ6AEwAHoECAkQAQ#v=one](https://books.google.com.ec/books?id=ufDefc0Kb1QC&pg=PA16&lpg=PA16&dq=H.+Mattoussiet++al.,J.++Appl.++Phys.83,+7965+(1998).&source=bl&ots=mzikSAFwhU&sig=ACfU3U2zKfMq7M0bIOy-VwDqYQxmND_WSw&hl=es&sa=X&ved=2ahUKEwikrd239ZrIAhWpmOAKHQ-ICxgQ6AEwAHoECAkQAQ#v=one)
46. Key enabling technologies | European Commission [Internet]. [cited 2019 Oct 22]. Available from: [https://ec.europa.eu/info/research-and-innovation/research-area/key-enabling-technologies\\_en](https://ec.europa.eu/info/research-and-innovation/research-area/key-enabling-technologies_en)
47. González JM, López M, Ruiz G. Informe de vigilancia tecnológica en nanomedicina. *Circ innovación en Biotecnol*. 2007;123.
48. Velásquez C. Nanopartículas: fundamentos y aplicaciones. *Nanotecnología Fundam y Apl*. 2015;203–22.
49. Bailey RE, Smith AM, Nie S. Quantum dots in biology and medicine. *Phys E Low-Dimensional Syst Nanostructures*. 2004;25(1):1–12.
50. Taurozzi JS, Hackley VA, Wiesner MR. Ultrasonic dispersion of nanoparticles for environmental, health and safety assessment issues and recommendations. *Nanotoxicology*. 2011;5(4):711–29.
51. Nireesha G, Divya L, Sowmya C, Venkateshan N, Niranjan Babu M, Lavakumar V. Lyophilization/Freeze Drying -An Review. *Ijntps*. 2013;3(4):87–98.
52. Worsfold PJ, Zagatto EAG. Spectrophotometry: Overview ☆ [Internet]. 3rd ed.

Reference Module in Chemistry, Molecular Sciences and Chemical Engineering. Elsevier Inc.; 2017. 1–5 p. Available from: <http://dx.doi.org/10.1016/B978-0-12-409547-2.14265-9>

53. Campbell D, Pethrick RA, White JR. Ultraviolet – visible spectroscopy. *Polym Charact.* 2018;58–66.
54. Katoch A, Bhardwaj R, Goyal N, Gautam S. Synthesis, structural and optical study of Ni-doped Metal-organic framework for adsorption based chemical sensor application. *Vacuum* [Internet]. 2018;158:249–56. Available from: <https://doi.org/10.1016/j.vacuum.2018.09.019>
55. Dutrow BL, Christine CM. X-ray Powder Diffraction ( XRD ) [Internet]. 2013 [cited 2020 Jan 17]. p. 1–4. Available from: [https://serc.carleton.edu/research\\_education/geochemsheets/techniques/XRD.html](https://serc.carleton.edu/research_education/geochemsheets/techniques/XRD.html)
56. Epp J. X-Ray Diffraction (XRD) Techniques for Materials Characterization [Internet]. *Materials Characterization Using Nondestructive Evaluation (NDE) Methods.* Elsevier Ltd; 2016. 81–124 p. Available from: <http://dx.doi.org/10.1016/B978-0-08-100040-3.00004-3>
57. Anton Paar. X-Ray diffraction (XRD) :: Anton Paar Wiki [Internet]. 2019 [cited 2020 Jan 5]. Available from: <https://wiki.anton-paar.com/en/x-ray-diffraction-xrd/>
58. Stefanaki E. <Electron Microscopy basics.pdf>. 2008;1–11.
59. Tang CY, Yang Z. Transmission Electron Microscopy (TEM). In: *Membrane Characterization* [Internet]. 2017 [cited 2020 Jan 6]. p. 145–59. Available from: <https://warwick.ac.uk/fac/sci/physics/current/postgraduate/regs/mpagswarwick/ex5/techniques/structural/tem/>
60. Ni C. Scanning Electron Microscopy (SEM). In: *Encyclopedia of Tribology* [Internet]. 2013 [cited 2020 Jan 8]. p. 2977–82. Available from: [https://serc.carleton.edu/research\\_education/geochemsheets/techniques/SEM.html](https://serc.carleton.edu/research_education/geochemsheets/techniques/SEM.html)
61. Nanakoudis A. What is SEM? Scanning electron microscope technology explained [Internet]. ThermoFisher Scientific. 2018 [cited 2020 Jan 9]. Available from: <https://blog.phenom-world.com/what-is-sem>
62. Scanning Electron Microscopy - Nanoscience Instruments [Internet]. [cited 2020 Jan 8]. Available from: <https://www.nanoscience.com/techniques/scanning-electron-microscopy/>
63. Shindo D, Oikawa T. *Analytical Electron Microscopy for Materials Science.* Analytical Electron Microscopy for Materials Science. Springer Japan; 2002.

64. Kutchko BG, Kim AG. Fly ash characterization by SEM-EDS. *Fuel*. 2006;85(17–18):2537–44.
65. García-Barrasa J, López-De-luzuriaga JM, Monge M. Silver nanoparticles: Synthesis through chemical methods in solution and biomedical applications. *Cent Eur J Chem*. 2011;9(1):7–19.
66. Sibiyá NP, Moloto MJ. Shape control of silver selenide nanoparticles using green capping molecules. *Green Process Synth*. 2017;6(2):183–8.
67. Kumar B, Smita K, Cumbal L, Debut A. Green synthesis of silver nanoparticles using Andean blackberry fruit extract. *Saudi J Biol Sci [Internet]*. 2017;24(1):45–50. Available from: <http://dx.doi.org/10.1016/j.sjbs.2015.09.006>
68. Zou J, Xu Y, Hou B, Wu D, Sun Y. Controlled growth of silver nanoparticles in a hydrothermal process. *China Particuology*. 2007;5(3):206–12.
69. Ahmed S, Saifullah, Ahmad M, Swami BL, Ikram S. Green synthesis of silver nanoparticles using *Azadirachta indica* aqueous leaf extract . *J Radiat Res Appl Sci [Internet]*. 2016;9(1):1–7. Available from: <http://dx.doi.org/10.1016/j.jrras.2015.06.006>
70. Kumashiro Y, Ohachi T, Taniguchi I. Phase transition and cluster formation in silver selenide. *Solid State Ionics*. 1996;86–88(PART 2):761–6.
71. Kristl M, Gyergyek S, Kristl J. Synthesis and characterization of nanosized silver chalcogenides under ultrasonic irradiation. *Mater Express*. 2015;5(4):359–66.
72. Patterson AL. The scherrer formula for X-ray particle size determination. *Phys Rev*. 1939;56(10):978–82.
73. Fernández-Díaz E, Espinoza-Martinez AB, Flores-Pacheco A, Ramírez-Bon R, Castillo SJ, Ochoa-Landin R. Synthesis and Characterization of Silver Selenide Thin Films by Chemical Bath Deposition and Ionic Exchange. *J Electron Mater*. 2019;
74. Amelia E. CARBOHIDRATOS.
75. Ajitha B, Divya A, Harish G, Sreedhara R P. The influence of silver precursor concentration on size of silver nanoparticles grown by soft chemical route. *Res J Phys Sci*. 2013;1(7):11–4.